CHAPTER 3

Dissociative Recombination of H_3^+ Ions with Electrons: Theory and Experiment

Rainer Johnsen[a] and **Steven L. Guberman**[b]

[a]*Department of Physics and Astronomy, University of Pittsburgh, Pittsburgh, PA 16260, USA*
[b]*Institute for Scientific Research, 22 Bonad Road, Winchester, MA 01890, USA*

Contents

Advances in Atomic, Molecular, and Optical Physics, Volume 57 © 2010 Elsevier Inc.
ISSN 1049-250X, DOI: 10.1016/S1049-250X(10)59003-7

Abstract

Four decades of experimental and theoretical studies of the dissociative recombination of the seemingly "simple" H_3^+ ions with electrons have often given strongly disagreeing results. The literature on the subject abounds in terms like *enigma* and *puzzles*, and several authors have asked if the "saga" is finally approaching a satisfactory ending. Fortunately, recent progress in theory and experiment has greatly reduced many of the apparent contradictions. In this review, we attempt to reconcile the remaining discrepancies, in particular those between beam experiments and those employing plasma afterglow techniques. We conclude that there are no true contradictions between those results if one examines the conditions under which the data were taken and includes effects arising from third-body-assisted recombination. The best available theoretical treatments of purely binary recombination now agree rather well with state-of-the-art ion-storage ring results, but we think that further refinements in the complex theoretical calculations are required before it can be said that the mechanism of the recombination is understood in all details and that the "saga" has truly come to an end.

1. INTRODUCTION

H_3^+, the simplest of all polyatomic molecular ions, consists of three protons arranged in an equilateral triangle, held together by two electrons. The physics and chemistry of this ion has occupied a special niche in the molecular physics community for many years, and it is a fair question to ask why it continues to be of interest today and what progress has been made in understanding its basic properties. The apparent simplicity of this ion makes it attractive as a test case for *ab initio* quantum-chemical calculations and that certainly has stimulated much theoretical work. A second important motivation comes from astrophysics: H_3^+ is perhaps the second most abundant molecular species (after H_2) in interstellar clouds, in the ionospheres of the outer planets, and plays a central role in determining the ionization balance and in building more complex ions that determine the physical properties in these star-forming regions (Herbst, 2007; McCall, 2006; McCall et al., 2002). While the ion is quite stable, the relatively small proton affinity of H_2 (4.2 eV) enables efficient proton transfer to other molecules. However, if H_3^+ ions recombine efficiently with electrons and dissociate into H_2 and/or H atoms in the process, the same species from which they were formed by several slow steps, the reaction chain is essentially terminated, and recombination limits the rate of molecule formation. The effect of H_3^+ on

the interstellar chemistry can be quite complicated and lead to bistable chemical evolutions, as has been discussed in detail by Pineau Des Forêts and Roueff (2000).

In this review, we focus on the dissociative recombination (DR) of H_3^+ ions with electrons, a process that can be symbolically represented as

$$\begin{aligned} H_3^+ + e^- &\rightarrow H + H + H \\ &\rightarrow H_2 + H \end{aligned} \tag{1}$$

Anticipating later discussions, we note that Equation (1) may be read either as representing an ion–electron binary collision or as a reaction equation that describes a more complex process in an ionized gas. We adopt the first interpretation but note that other electron–ion recombination mechanisms exist in which part of the energy released by recombination is transferred to third bodies (atoms, molecules, or other electrons) or is removed by emission of radiation. We will discuss such third-body-assisted recombination only to the extent that it affects the interpretation of experimental data.

All experimental studies of DR face the problem that two charged species, ions and electrons, must be brought together in a controlled manner with a small relative velocity. Theorists have an equally and perhaps even more difficult task. A slow electron that is captured by a molecular ion can give rise to numerous excited states of the molecule, and it requires extensive quantum mechanical calculations to decide which of those states eventually lead to dissociation. The task is further complicated by the fact that recombination is sensitive to the rotational and vibrational states of the ion and that the ion exists in two nuclear spin modifications, denoted as para-H_3^+ (two of the three proton spins aligned) and orho-H_3^+ (three proton spins aligned).

As in other fields of physics and chemistry, experiment and theory sometimes have often given conflicting answers to some of the basic questions. For many years there was considerable doubt that efficient recombination of H_3^+ actually occurred! Many open and once difficult questions have been clarified in recent years by advances in theory and by new and powerful experimental techniques, especially ion-storage rings that supply more detailed information than the plasma-based experimental methods. Progress in theory has been commensurate with that in experiment: what Bates (1993), the "founding father" of DR, once described as an "enigma" has largely been solved, but some finer details may still need to be worked out.

This review is intended to present a critical but not necessarily complete analysis of all experiments and theories. We seek to reconcile experiment and theory as far as possible given the current state of knowledge, and to see if remaining discrepancies are "real" in

the sense that they indicate deficiencies in our understanding as opposed to incomplete or erroneous interpretations of experimental observations.

The literature on DR is extremely large and H_3^+ is certainly not the only ion of interest. Several excellent reviews on DR in general have appeared in the last few years that include extensive lists of measured rate coefficients and other data (Florescu-Mitchell & Mitchell, 2006; Larsson & Orel, 2008). A previous review of H_3^+ recombination measurements by Johnsen (2005) contains much additional material that we will not repeat here, and some proposed solutions of apparent contradictions have now been ruled out by new experimental and theoretical work.

2. BASIC DEFINITIONS

We begin by reviewing some basic definitions, most of which are common in the physics of atomic collisions, but others are specific to particular experiments and require a few words of explanation.

Consider an ion that moves in a region containing uniformly distributed free electrons at density n_e (cm^{-3}). The recombination coefficient α is defined by the probability dP that the ion captures an electron during time dt and dissociates before releasing it by autoionization, i.e.,

$$dP = \alpha n_e dt. \tag{2}$$

This defines a "raw" or "effective" recombination coefficient that still depends on the distribution of the relative ion–electron speeds $f(v_{rel})$. If the recombination is purely binary, one can define a recombination cross section $\sigma(v_{rel})$, which is related to the rate coefficient by the average

$$\alpha = \langle \sigma(v_{rel}) v_{rel} f(v_{rel}) \rangle, \tag{3}$$

where the brackets indicate averaging over all v_{rel}. If $f(v_{rel})$ is sufficiently narrow to be reasonably approximated by a delta function centered at $<f(v_{rel})>$, the cross section is closely given by the ratio

$$\sigma(v_{rel}) \cong \frac{\alpha}{\langle v_{rel} \rangle}. \tag{4}$$

This approximation is fairly good in merged-beam experiments, but fails at very low v_{rel}. For that reason merged-beam experimenters often report their raw results not as cross section but as a nonthermal recombination coefficient as a function of the "detuning energy." However, they usually deconvolute the recombination coefficient to obtain the cross section, and then compute the thermal recombination coefficient by

convolving the cross section again with a Maxwell distribution. The deconvolution may require extrapolation to very low energies.

Plasma afterglow experiments directly yield the thermal recombination coefficient, although often only over a narrow range of temperatures. Those results are typically given in the form of a power-law dependence

$$\alpha(T_e) = \alpha(300K)\left(\frac{T_e}{300}\right)^{-x}, \tag{5}$$

as a function of the electron temperature T_e. In such experiments, the ion translational ion temperature T_i is almost always the same as the gas temperature T_g, but T_e can be greater than T_i. It can hardly ever be assumed that the internal degrees of freedom of the ions, especially their vibrations, are in thermal equilibrium at the translational temperature.

Theoretical calculations usually generate cross sections for a set of discrete collision energies. To facilitate comparison to experiment, theorists often calculate (a) the thermal rate coefficient and (b) an "effective" rate coefficient that should be measured in beam experiments with a finite energy resolution. The procedure "washes out" some of the finer structure in the theoretical cross section but, unlike the thermal rate coefficient, retains some of its structure.

3. EXPERIMENTAL TECHNIQUES

The experimental techniques used to study DR can be divided into two broad categories, plasma afterglow experiments and merged-beam experiments.

In afterglow experiments, electron–ion recombination rate coefficients and product yields are derived from observations of ion and electron densities, optical emissions, and neutral products during the afterglow phase of a plasma. The analysis of afterglow plasmas can be complicated by reaction processes that occur in addition to electron–ion recombination, and it also is not always obvious that recombination in a plasma involves only simple binary recombination. However, what is regarded as a "complication" in the context of recombination may be of great interest to the physics of ionized gases in general and this should be kept in mind.

Merged-beam and ion-storage ring methods, while requiring far greater experimental effort, are closer to the theorists' ideal experiment and can provide more detailed information. The outstanding progress that has been made in refining these techniques now permits studies with very high energy resolution as well as determinations of the chemical

identity of neutral reaction products and their kinetic energy. Such data, of course, provide far more sensitive tests of theoretical calculations of recombination than the thermally averaged rate coefficients obtained by afterglow techniques.

3.1 Afterglow Techniques

The two principal subcategories, "stationary" or "flowing" afterglows, have much in common, but they differ in the way that the plasma is produced and observed. We will discuss them together while pointing out relative strengths and weaknesses.

In the stationary afterglow, more appropriately called a "pulsed" afterglow, a plasma in a pure gas or gas mixture is created by repeated pulses of microwaves, high voltages applied to discharge electrodes, ultraviolet light, or other ionizing radiation (see Figure 1). All afterglow observations are carried out in the same volume as a function of time.

In the flowing afterglow method (see Figure 2), a pure gas (helium most often) is first ionized, usually in a microwave discharge, and then flows at high speed down the flow tube and is eventually discharged into a fast pump. At some point, reagent gases are added that convert the primary ions and metastable atoms to the desired molecular ion species. Recombination occurs in the region downstream from the reagent inlet, and observations are carried out as a function of distance from the gas inlet. The flow tube method has the advantage of greater chemical flexibility and it avoids exposing the molecular gases directly to an intense discharge, which can lead to undesired excitation or dissociation. It also has some disadvantages: There is only an approximate correspondence between time and distance since the gas flows faster at the center of the tube than it does near the wall and the spatial distribution of particles in the plasma is not necessarily uniform. Also, the mixing of gases at the reagent inlet is not instantaneous and this can complicate the data analysis.

A frequently employed method to convert the active species flowing out of the discharge to ions consists of adding argon at a point upstream from the reagent inlet. This converts metastable helium to argon ions, which are subsequently used as precursors for the ion–molecule reactions that generate the desired ion species. What is often ignored is that along with the argon ions some undesired energetic particles and ultraviolet photons also enter the region downstream from the reagent inlet, for instance metastable argon atoms (see, e.g., Skrzypkowski et al., 2004) that are produced by collisional radiative recombination of argon ions. Ultraviolet photons, in particular "trapped" helium resonance radiation, can enter the reaction zone unless one adds a sufficient amount of argon to destroy them by photoionization of argon. Fortunately, such effects do

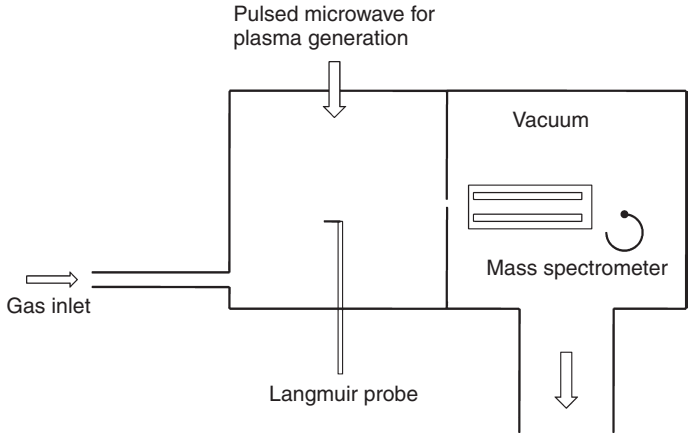

Figure 1 Schematic diagram of a stationary or pulsed afterglow apparatus. A Langmuir probe or a microwave frequency method is used to record the decay of the electron density subsequent to an ionizing pulse. Typical linear dimensions of the plasma chamber are 10–40 cm

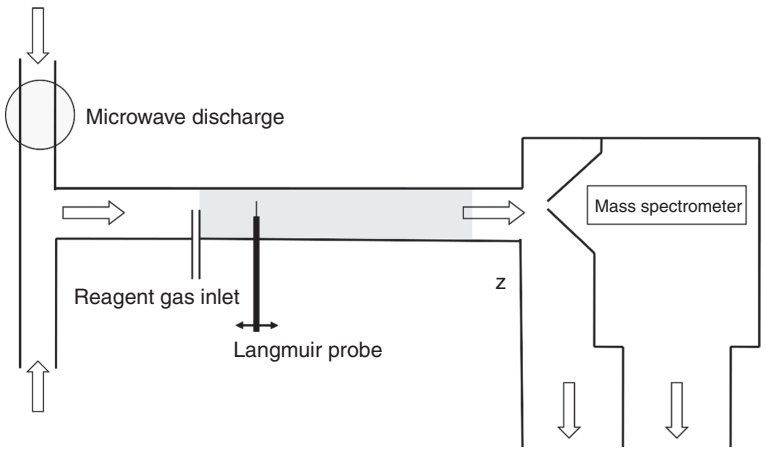

Figure 2 Schematic diagram of a flowing afterglow Langmuir probe apparatus (FALP). A movable Langmuir probe records the electron density as a function of distance from the reagent inlet

not interfere much with measurements of recombination coefficients, but they can be important in spectroscopic studies of reaction products.

Different afterglow experiments employ different reaction sequences to produce H_3^+ ions. One frequently used scheme makes use of the fast two-step reaction sequence

$$Ar^+ + H_2 \rightarrow ArH^+ + H + 1.53eV \quad (6)$$

followed by

$$ArH^+ + H_2 \rightarrow Ar + H_3^+ + 0.57eV \quad (7)$$

which releases sufficient energy to produce $H_3{}^+$ in vibrational states up to $v = 5$. If argon is present in sufficient concentration, subsequent proton transfer to Ar,

$$H_3^+(v) + Ar \rightarrow ArH^+ + H_2, \quad (8)$$

destroys all $H_3{}^+$ ions with internal energies above 0.57 eV, leaving only those in the ground state [A_1 (0, 0^0)], in the $v_2 = 1$ bending-mode vibration [E (0, 1^1) at 0.3126 eV], and in the $v_1 = 1$ breathing-mode vibration [A_1 (1, 0^0) at 0.394 eV]. The radiative lifetime of the $v_1 = 1$ state is very long (~1.2 s). Radiative decay of ions in the $v_2 = 1$ level is faster (~4 ms), but does not necessarily occur at the time scale of recombination measurements.

The electron density can be measured by several methods: Langmuir probes return local values of n_e, while microwave methods have low spatial resolution and yield a "microwave-averaged electron density."

The flow tube has the significant practical advantage that the gas is exchanged rapidly, on a time scale of milliseconds. In stationary afterglows, outflow of gases occurs only through the small sampling orifice used for mass spectrometric sampling of ions, but the gas exchange time is usually on the order of many minutes. For this reason, impurity problems tend to be less serious in flow tubes than in stationary afterglows.

The methods to measure recombination coefficients are essentially the same in both types of afterglows. In the simplest case, when only a single ion species is present and the plasma is quasi-neutral, e.g., $n_e = n_i$, the electron continuity equation is given by

$$\frac{\partial n_e(t, \vec{r})}{\partial t} = -\alpha n_e^2(t, \vec{r}) + D_a \nabla^2 n_e(t, \vec{r}), \quad (9)$$

where D_a is the ambipolar diffusion coefficient of the ion. If diffusion is sufficiently slow that it can be ignored, the reciprocal electron density varies with time as

$$\frac{1}{n_e(t, \vec{r})} = \frac{1}{n_e(0, \vec{r})} + \alpha t, \quad (10)$$

and hence the recombination coefficient can be obtained directly from the slope of a graph of the measured reciprocal electron densities as a function of time. This simple form of analysis yields reasonably accurate

recombination coefficients only if the diffusion current of ions into or out of the volume in which n_e is measured is very small compared to the volume loss rate of electrons due to recombination. A frequently used, but not entirely satisfactory, approximation "corrects" for the diffusion loss of electrons by fitting the observed electron density decays to an equation of the form

$$\frac{dn_e(t)}{dt} = -\alpha n_e^2(t) - \frac{D_a n_e}{\Lambda^2}, \tag{11}$$

in which Λ^2 is the fundamental diffusion length of the plasma container, and the electron density is measured at the center of the container (or points on the axis of a flow tube). The equation is correct only in the limits when either of the two loss terms greatly outweighs the other since it ignores the fact that quadratic recombination loss tends to "flatten" the spatial distribution of electrons and ions. As a consequence, the diffusion current away from the center is reduced, and Equation (11) overestimates the diffusion loss, but underestimates the recombination loss. The pulsed microwave afterglow measurements often employed numerical solutions of the continuity equations to analyze the data while the analysis of flow tube data is usually carried out using Equation (11).

The time scale of recombination experiment is of practical interest. From Equation (10), it follows that the electron density during the afterglow decays by a factor of 2 from its value at time t whenever the time increases by the "half-time" $\tau_{1/2}$, given by

$$\tau_{1/2} = \frac{1}{\alpha n_e(t)}. \tag{12}$$

Accurate determinations of recombination coefficients require observation of n_e over a significant range, a factor of 4 or preferably more. Hence, for an initial electron density of $n_e(t=0) = 10^{10}$ cm^{-3} and a typical recombination coefficient $\alpha = 10^{-7}$ cm^3/s, one must measure $n_e(t)$ over a time of at least $(1+2) = 3$ ms, longer if the initial electron density is only 10^9 cm^{-3}. Obviously, the ion–molecule reactions that form the desired ions should go essentially to completion in a time short compared to the time scale of recombination, and the ions under study must not convert to a different type during this time by reacting with any of the gases in the afterglow plasma or impurity gases. We will show later (see Section 6.1) that serious errors ensue when these requirements are not fulfilled.

The gas temperature in afterglows can be adjusted fairly easily over a limited range from liquid-nitrogen temperature (77 K) to roughly 600 K by heating the entire apparatus. This is more useful as a means to control equilibrium concentrations of weakly bound ions (for instance shifting the chemical equilibrium from H_3^+ to H_5^+ ions) than as a means to measure the

temperature variation of recombination coefficients. Much higher electron temperatures (up to 10,000 K) can be reached by microwave heating of the electron gas, a technique that was used extensively in stationary afterglows and that has provided data on many important ion species, including H_3^+. The technique is subject to complications in the presence of molecular additives (Johnsen, 1987). In the afterglow measurements on H_3^+, such effects are not important and we will not discuss this subject further.

Higher gas temperatures (up to nearly 10,000 K) can be reached by employing shock heating of the afterglow plasma (Cunningham et al., 1981), a technique that has been applied to several recombination processes of atmospheric interest but not to H_3^+.

3.2 Single-Pass Merged-Beam and Ion-Storage Ring Experiments

With the development of ion-storage rings, experiments on DR were transformed from small-scale "table-top" experiments to large-scale multiuser type operations that made use of technologies from nuclear and high-energy physics. The impact of these new machines cannot be overstated: the considerable investment in the experimental facilities revitalized and revolutionized experimental studies of DR. We will only summarize the basic principles and current capabilities since extensive reviews have been written by authors who are more familiar with experimental details (Larsson & Orel, 2008).

The predecessor of the storage rings, the single-pass merged-beam method was developed at the University of Western Ontario (see, e.g., Auerbach et al., 1977). While it was an important step forward and resulted in many important results, the single-pass merged beam has been superseded by the more powerful ion-storage ring technique. Both have in common that recombination of ions and electrons takes place between parallel ion and electron beams of nearly the same velocity. In a single-pass merged beam, the ion beam passes through the electron target beam once and is then discarded; in a storage ring the ions circulate in the ring and pass through the interaction region (see Figure 3) many times. It is not the more "efficient" use of ions in storage rings that makes them preferable but the fact that the longer storage time (up to 10 seconds) in a ring removes all excited ions that radiate on that time scale, for instance infrared active vibrationally excited ions.

In merged beams, the relative velocity between the two beams can be made very small. More importantly, the velocity spread in the electron target gas can be greatly reduced by accelerating the (initially "hot") electrons to a high velocity that closely matches that of the ions. The narrowing of the electron velocity distribution in the direction of the beam (but not transverse to it) is a purely kinematic effect that follows from the classical equations of motion. However, at finite electron

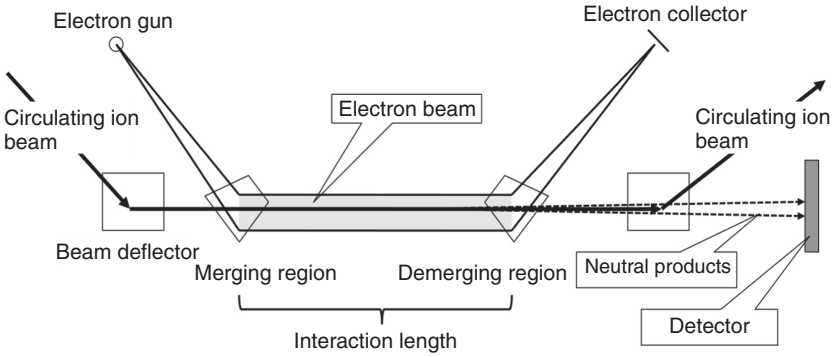

Figure 3 Schematic diagram of the electron cooler and interaction region of an ion-storage ring. The length of the interaction region is typically on the order of 1 m

densities Coulomb interactions between electrons occur and the actual velocity spread in the beam direction is somewhat larger than that calculated from the kinematic equations. In addition, the effective energy resolution for ion–electron collisions depends also on the velocity components transverse to the beam. It is common practice to model the electron velocity distribution by a two-temperature Maxwellian function with temperatures $T_{\parallel}$ for the parallel velocity component and $T_{\perp}$ for the two transverse components.

Several methods are available to reduce the transverse velocity spread and thereby improve the energy resolution: In the single-pass merged-beam apparatus (Auerbach, 1977), improvements in the energy resolution were made by using trochoidal analyzers to merge electron and ion beams, while storage rings employ "electron coolers" in which the electrons are cooled by expansion in a magnetic guiding field. Cooling and recombination can be accomplished either in the same section of the ring or in the two separate sections. In addition, the coolers also cool the ion beam by a "friction" effect and reduce the diameter of the ion beam.

In all merged-beam techniques, recombination events are detected by counting recombination products using an energy-sensitive barrier detector. The detector ideally registers one count of full pulse height when all products from a single event strike the detector simultaneously. In that case the number of counts received for a single traversal of a single ion through the electron target is

$$N = \alpha n_e \Delta t. \tag{13}$$

Here α is the recombination rate coefficient appropriate to the experimental velocity distribution, n_e the electron density, and Δt the time of traversal of an ion through the interaction region. If the ion beam is much narrower than the electron beam, which is the case in storage rings, there

is no need to consider overlap factors. To obtain absolute values of α, one needs to know the ion beam current, which can be measured either by collecting ions or using a current transformer.

While ion-storage rings come very close to the theorist's perception of an ideal experiment, there are some, fortunately minor, imperfections that should be mentioned. Ion–electron collisions also occur in the merging and demerging regions (magnets in storage rings) where the ion and electron beams are obviously not parallel and their relative velocities are larger than those in the straight part of the interaction region; however, this "toroidal correction" is not large and can be taken into account.

In addition to providing high-resolution recombination cross sections, storage rings have an outstanding ability to determine the relative abundance of recombination products by placing grids in front of the detector and analyzing the pulse-height spectra (for details, see Larsson & Orel, 2008). The single-pass merged beam also has been employed for such studies but the small event rate made quantitative product determinations tedious and time consuming.

4. THEORY

4.1 DR Mechanisms

If all internuclear distances in a polyatomic molecule are held constant except for the dissociation coordinate, a potential curve similar to that for a diatomic molecule can be used to illustrate the fundamental features of DR. Figure 4 shows such a slice through the potential surfaces of the ion, Rydberg, and dissociative states. ϵ denotes the electron energy at which capture takes place into a repulsive state of the neutral molecule from an ion in some vibrational level. Note that any electron energy will do, even zero, since varying the electron energy only varies the point of capture. Once in the repulsive state, the neutral molecule can emit the captured electron or dissociate. If dissociation takes the internuclear distance beyond the crossing point of the neutral and ion curves, electron emission (autoionization) is no longer possible and dissociation is completed. This is the direct mechanism for DR originally proposed by Bates (1950). Superexcited states of the neutral molecule are generally found at the same total energies as that for the ion ground state. Electron capture also occurs into these superexcited states and competes with capture into the dissociative state. Among these states are the vibrationally excited Rydberg states that have the ground state of the ion as core. The $v=0$ ground core Rydberg levels all lie below the ion, but the $v=1$ ion level is the energetic limit of an infinite number of Rydberg levels as are the other excited ion vibrational levels. Capture into one of these levels at electron

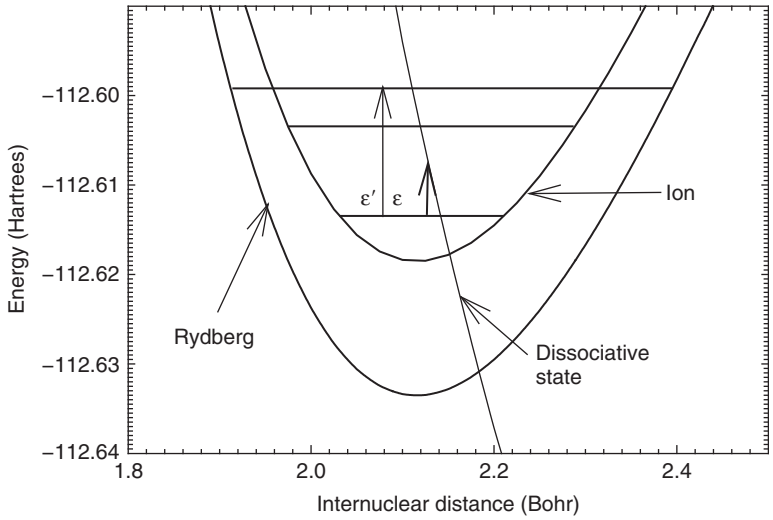

Figure 4 The direct (at electron energy ε) and indirect (at electron energy ε') mechanisms of dissociative recombination

energy ε' is shown in Figure 4. After capture, the electron can be emitted or the Rydberg level can be predissociated by the dissociative state of the direct mechanism. This is the indirect DR mechanism, first introduced by Bardsley (1968). Both the direct and indirect mechanisms are paths to the same dissociation products and can interfere with each other. Any technique for calculating the DR cross section must account for this interference. A recent addition to the indirect DR mechanism, Rydberg states having an excited ion core (Guberman, 2007), will not play a role in H_3^+ DR at low electron energies since the first excited ion states lie too high above the ground state (Shaad & Hicks, 1974). A second-order mechanism (Guberman & Giusti-Suzor, 1991; Hickman, 1987; O'Malley, 1981) also can take place in which the neutral repulsive state acts as an intermediate between the electron–ion and a bound Rydberg state. In this manner, an electron can be captured by an electron–electron interaction into a Rydberg state.

4.2 H_3^+ Potential Curves and Surface

Figure 6 has potential curves for H_3^+ and for several H_3 states that are important for DR. These states have been calculated in C_{2v} symmetry with the nuclear configuration shown in Figure 5, i.e., R_1, the distance between two H atoms has been kept constant at the equilibrium separation, 1.63 a_0. The remaining atom moves along R_2, which is perpendicular

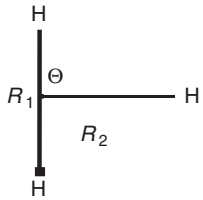

Figure 5 Jacobi coordinates for H_3

to R_1 and intersects R_1 at its midpoint. The potential curves are calculated with [4s, 3p, 2d, 1f] Gaussian basis sets centered on each H atom. For the description of Rydberg surfaces, this basis set is supplemented with six diffuse s and six diffuse p basis functions placed at the center of mass. Orbitals are determined in Hartree-Fock (HF) calculations on H_3^+, and the final energies are obtained from CI wave functions calculated by taking all single and double excitations to the virtual orbitals from a large reference set of configurations. The potential curves are identified by the symmetries in C_{2v} as well as the symmetries at the equilateral triangle configuration in D_{3h}. It is clear from Figure 6 that no neutral state potential curves cross the X^1A_1 ground-state ion curve ($X^1A'_1$ at the equilateral triangle configuration), the highest potential curve in the figure. The two possible dissociative routes are the lowest curves, 1^2A_1 and 1^2B_2. These curves are degenerate at the equilateral triangle position where they have $1^2E'$ symmetry, and they have asymptotes that lie below

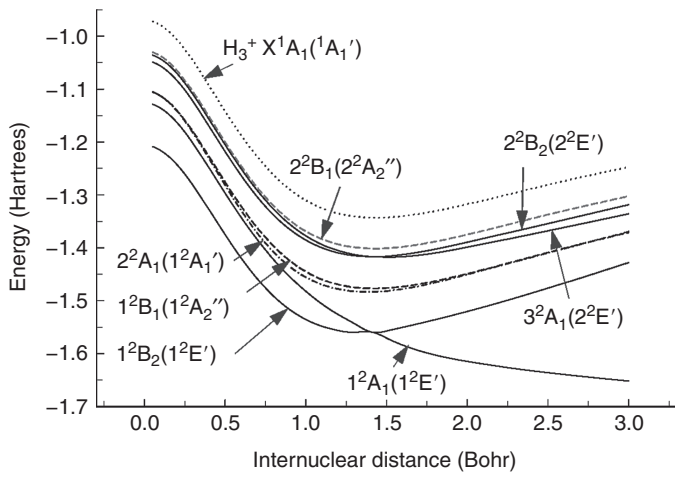

Figure 6 Potential curves for the approach of one H in C_{2v} geometry along R_2 (as in Figure 5) to the midpoint of the other two H atoms held at $R_1 = 1.63$ a_o

the ground vibrational state of H_3^+. No other states can provide DR routes at low electron energies. These states consist of a 2px or 2py orbital bound to the ion ground state where the *xy* plane is the plane of the molecule. Because these states do not cross the ion, DR was initially thought to be slow for H_3^+. This is discussed further below. The neutral curves shown in Figure 6 are qualitatively similar to those shown in Figure 3 of Petsalakis et al. (1988). A precise comparison is not possible due to the different geometries used in their figure. However, at the equilateral triangle geometry, the curves in Figure 6 are about 0.12 eV lower than those of Petsalakis et al. (1988).

Also shown in the figure are the 3^2A_1 and 2^2B_2 states, which are the components of the $2^2E'$ doubly degenerate state at the equilateral triangle configuration. These states are too high in energy to be dissociative channels at low electron energies.

Figure 7 shows a two-dimensional surface for 1^2A_1, 1^2B_2 and the ion ground state. In the plot, both R_1 and R_2 are varied and Θ, as shown in Figure 5, is fixed at 90°. Both neutral surfaces intersect at the equilateral triangle configuration. As shown in the figure, the 1^2A_1 surface leads to $H_2 + H$ and both 1^2A_1 and 1^2B_2 can generate $H + H + H$.

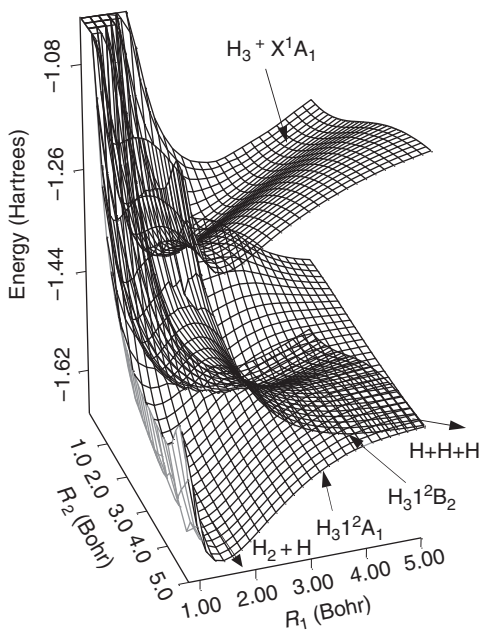

Figure 7 Potential surfaces for H_3 and H_3^+ using the coordinates of Figure 5 with $\Theta = 90°$

4.3 Vibrational and Rotational Considerations

The nuclear configuration of the ground state of H_3^+ is an equilateral triangle and belongs to symmetry group D_{3h}. The normal modes are shown in Figure 8, labeled using the notation of Herzberg (1945). The first normal mode, labeled ν_1, is the symmetric stretch or breathing mode. The remaining normal modes, ν_{2a} and ν_{2b}, are degenerate, i.e., they have the same frequency. Indeed, ν_{2a} and ν_{2b}, as shown in Figure 8, are not unique. An infinite number of pairs of modes can be obtained by taking orthogonal linear combinations of ν_{2a} and ν_{2b}, and they are all equally valid. If one degenerate mode is superposed upon another with different phases for the vibrational motion, the H atoms will move in ellipses (Herzberg, 1945). If the motion in the two modes is out of phase by 90° (i.e., when the atoms in one mode are passing through the equilibrium position, the atoms in the other mode are at the maximum displacement), the H atoms will move on circles and the motion can be described with a vibrational angular momentum quantum number, ℓ. Instead of describing the vibrational state of the molecule with quantum numbers, v_1, v_2, and v_3, it is now common practice to use (v_1, v_2^{ℓ}). For H_3^+ (Watson, 2000), $\ell = -v_2, -v_2+2, \ldots, v_2 - 2, v_2$.

Since H_3^+ is a symmetric top (i.e., two of its moments of inertia are equal), the quantum numbers specifying the rotational energy levels are N^+, the total angular momentum, and K^+, the projection of N^+, upon the molecular symmetry axis. Each proton has a spin of 1/2 and the total nuclear spin, I, can be 3/2 (ortho) or 1/2 (para). For the ortho states, $K^+ = 3n$, where n is an integer (Pan & Oka, 1986). For the para states, $K^+ = 3n \pm 1$ (Pan & Oka, 1986). It can be shown that the state with (N^+, K^+) = (0, 0) does not exist. The lowest energy rotational state is for (1, 1) and is para. The second level, at 23 cm^{-1} above (1, 1), is (1, 0) and is ortho. The (1, 0) level is highly metastable since an ortho–para transition is forbidden. The lowest ortho levels are (1, 0), (3, 3), (3, 0), and (4, 3). The lowest para levels are (1, 1), (2, 2), (2, 1), and (3, 2). It is interesting to note, especially for the

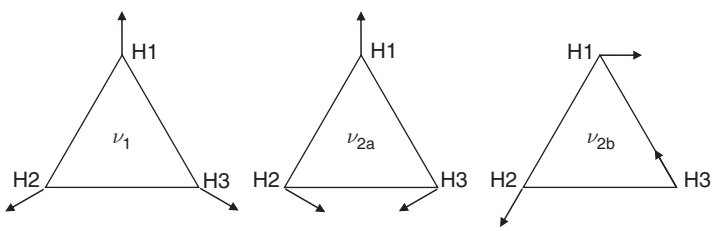

Figure 8 The three normal mode vibrations of the ground state of H_3^+

interpretation of DR experiments, that all of these levels have very long lifetimes (Pan & Oka, 1986). The radiative lifetimes are 1.2×10^6 seconds for (2, 2), 15×10^6 seconds for (2, 1), 3.3×10^4 seconds for (3, 2), 2.2×10^4 seconds for (3, 0), and 2.2×10^4 seconds for (4, 3) (Pan & Oka, 1986). Once generated, these ions will not decay by photoemission during DR experiments.

4.4 One- and Two-Dimensional Theory

4.4.1 Direct Recombination

The direct recombination cross section for vibrational level v', $\sigma_{v'}$, is given by (Bardsley, 1968; Flannery, 1995; Giusti, 1980)

$$\sigma_{v'} = \frac{2\pi}{k^2} r \frac{\Gamma_{v'}}{(1 + \Sigma_v \Gamma_v)^2} \tag{14}$$

where $\Gamma_{v'} = \pi^2 |(\Psi_d X_d | H | \Psi_i X_{v'})|^2$, r is the ratio of the statistical weights of the neutral and ion states, k is the wave number of the incident electron, v runs over the open ion vibrational levels, X_d and $X_{v'}$ are dissociative and bound vibrational wave functions, respectively, Ψ_d and Ψ_i are electronic wave functions of the dissociative and the ion states, respectively, and H is the electronic Hamiltonian. Equation (14) does not account for the intermediate Rydberg levels. In the expression for $\Gamma_{v'}$, the integration is over the electronic and nuclear coordinates. If the dissociative potential curve does not cross within the turning points of the ion vibrational level, the small vibrational overlap will lead to a small $\sigma_{v'}$. Figure 6 shows that the dissociative potential curves, 1^2A_1 and 1^2B_2, in a one-dimensional view, do not cross the ion. This feature alone led theorists (Kulander & Guest, 1979; Michels & Hobbs 1984) to predict that the DR rate constant for H_3^+ is small. At the time, the direct recombination process was thought to be much more important than the indirect process.

4.4.2 Multichannel Quantum Defect Theory

Because of the large literature on Multichannel Quantum Defect Theory (MQDT), a full description of the technique is not given here. Instead we guide the reader to the most relevant literature. The primary advantages of MQDT for the study of DR is that one can account for interference between direct DR and indirect DR with both being treated equally and one can treat entire Rydberg series rather than concentrating upon individual states as would be the case with a scattering theory approach. The pioneering studies which introduced MQDT to the study of DR were those of Lee (1977) and Giusti (1980). The approach of Giusti (1980) modified by Nakashima et al. (1987) to incorporate Seaton's (1983) closed-channel

elimination procedure for the *S* matrix is the approach used today by most theorists. The theory involves a *K* or reaction matrix which contains the interaction matrix elements between all channels. The *K* matrix is calculated perturbatively from the Lippmann–Schwinger equation. The first papers used a *K* matrix limited to first order. The usage of a second-order *K* matrix was introduced by Guberman and Giusti-Suzor (1991). The original approach has been revised to include rotation (Schneider et al., 1997; Takagi, 1993; Takagi et al., 1991), derivative couplings (Guberman, 1994), Rydberg states with excited cores (Guberman, 2007), and spin–orbit coupling (Guberman, 1997). An excellent reference on MQDT is the volume by Jungen (1996) and the papers contained therein.

4.4.3 Dissociative Recombination of HeH^+ and One-Dimensional H_3^+

A clue that the theoretical view of H_3^+ could be wrong came in calculations on a diatomic molecule that shares the noncrossing features of H_3^+. Because we can think of HeH^+ as H_3^+ with two of the protons superposed, they are expected to have similar recombination mechanisms. Figure 9 shows the ground-state potential curve for HeH^+ and curves for seven HeH states (Guberman, 1994, 1995). All the HeH states in Figure 9 are Rydberg with the exception of the ground state. None of the states cross the ion curve. For this case, it was shown that electron capture could occur by breakdown of the Born–Oppenheimer principle, which also drives indirect DR. Because all the states found to be involved in DR are adiabatic Rydberg states, there are no electronic couplings between these states. Instead, derivative couplings were introduced to drive DR between the adiabatic states. The cross section was calculated for ^{3}HeH up to 0.3 eV, using the MQDT approach (Giusti, 1980; Guberman & Giusti-Suzor, 1991), and over most of this region, the indirect process was much more important than direct recombination. Indeed, inclusion of the indirect mechanism increased the cross section by a factor of 49 (Guberman, 1995). For ^{3}HeH, it was also found that He + H(2s) are the main dissociation products at low electron energies. The total rate coefficient at 300 K was 2.6×10^{-8} cm^3/s, giving a clear example of how DR, dominated by the indirect mechanism, can have a high rate coefficient. Indeed, the rate would have been higher if it had been calculated for the true analog of H_3^+, the unphysical ^{2}HeH. The potential curves shown in Figure 8 apply also to ^{2}HeH, but the lower mass, compared to ^{3}HeH, raises the vibrational levels in the well leading to higher overlap with the $C^2\sum^+$ dissociative state. Other calculations (Sarpal et al., 1994) for ^{4}HeH using an *R*-matrix approach did not report a rate coefficient but also found that indirect recombination dominated the cross section. The main dissociation products were He + H (1s) at low electron energies. This was surprising since the identity of the dissociation products found

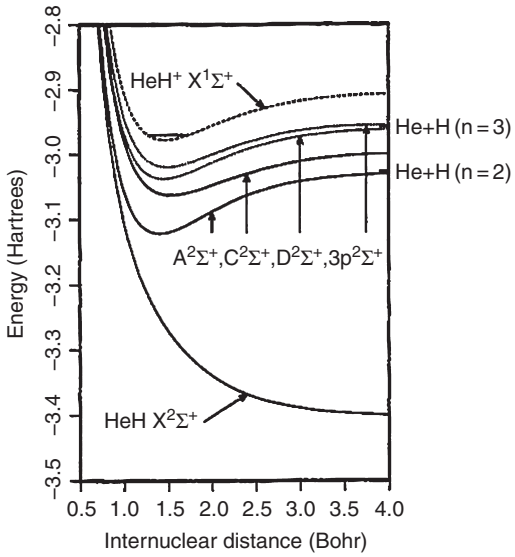

Figure 9 Potential curves for HeH and HeH^+ from Guberman (1995). Reprinted by permission from the AIP Press

with the MQDT approach was a qualitative and not a quantitative result. Experiments (Strömholm et al., 1996) have since verified that the main products are He + H (2s).

Takagi (2003) reported a one-dimensional MQDT treatment of DR using the potential curves of Michels and Hobbs (1984). He found that the rate coefficient of the recombining ion was highly sensitive to the initial rotational level with the $N \geq 4$ levels of the vibrational ground state having large rate coefficients.

4.4.4 Derivative Couplings for H_3^+

In a study of the predissociation of H_3 (Schneider & Orel, 1999), d/dR_1 and d/dR_2 (see Figure 5 in their paper) derivative couplings connecting the lowest $^2A_1$ dissociative state with $2s^2A_1$ and $3s^2A_1$ were reported. For the 2s state, the d/dR_1 coupling at the ion equilibrium separation ($R_1 = 1.65$ a_o and $R_2 = 1.43$ a_o) is 0.15 a_o^{-1} and that for d/dR_2 is –0.20 a_o^{-1}. (The phase of the coupling is arbitrary since it depends upon the phases of the orbitals and the total wave function.) The largest d/dR_1 coupling is 0.75 a_o^{-1} at $R_1 = 1.15$ a_o^{-1} and $R_2 = 0.92$ a_o^{-1} and for $|d/dR_2|$ it is >0.95 near $R_1 = 1.15$–1.85 and $R_2 = 0.93$. The largest coupling in this case is for R_1 near the equilibrium separation but for R_2 smaller than the equilibrium separation. The couplings with the 3s Rydberg state, as

expected, are much smaller. Tashiro and Kato (2002) have reported derivative couplings calculated in hyperspherical coordinates between the two 2pE′ (1^2A_1 and 1^2B_2 states in C_{2v}) dissociative states and the $2s^2A_1$. They found a large coupling that peaks at 5 a_o^{-1} for a hyperradius of 1.5 a_o and hyperangles of $\theta = 1/2$ and $\phi = \pi/6$ radians and for the upper 2pE′state (1^2B_2). Couplings with the lower 2pE′ state (1^2A_1) were found to be much smaller in agreement with the results of Schneider and Orel (1999).

4.4.5 Two-Dimensional Cross Sections

Using a combined wave packet MQDT approach and derivative couplings, a two-dimensional calculation (varying R_1 and R_2 as in Figure 5) was performed for DR along the $^2B_2$ surface (Schneider et al., 2000). For direct recombination, they found that the calculated cross section is 4–5 orders of magnitude below the experimental cross section (Larsson et al., 1997). However, the inclusion of Rydberg states coupled together by the R_1 and R_2 dependence of the quantum defect led to a dramatic increase in the cross section although the theory was still two orders of magnitude less than the experimental cross section. The authors concluded that the Rydberg channels, via the indirect mechanism, played a crucial role in the DR of H_3^+. They attributed the difference between theory and experiment to the lack of a full three-dimensional treatment and to the absence of the $^2A_1$ dissociative state in the theoretical treatment. They also tested the proposal of Bates that DR in H_3^+ may occur via interconnected Rydberg states in which the connection is mainly between states differing by $\Delta v = 1$. They found that $\Delta v \geq 1$ connections are also very important.

4.5 Three-Dimensional Treatments of H_3^+ DR

The first three-dimensional theoretical treatment of the DR of a polyatomic molecule (Kokoouline et al., 2001) combined several new theoretical methods for the study of DR with aspects of the MQDT approach. In these pioneering calculations, a new driving mechanism, not present in diatomic molecules, was introduced. The next section contains a brief description of the adiabatic hyperspherical approach. Section 4.5.2 describes the role of Jahn–Teller (JT) coupling in the DR of H_3^+. Section 4.5.3 summarizes the role of the nuclear spin. The approach to calculating the cross sections used in the first paper (Kokoouline et al., 2001) is given in Section 4.5.4. The revised approach used in later papers is discussed throughout and described further in Section 4.5.5. The last section contains suggestions for future theoretical research.

4.5.1 Hyperspherical Coordinates and the Adiabatic Approximation

The calculations describe the nuclear motion with hyperspherical coordinates consisting of a hyperspherical radius, R, and two hyperangles, θ and ϕ. The coordinates can be defined in terms of the distances between the H atoms. Taking r_i to be the distance between atom i and the center of mass, the hyperradius is given by $R^2 = \sqrt{3}\ (r_1{}^2 + r_2{}^2 + r_3{}^2)$ (Kokoouline et al., 2001). In later papers (Kokoouline & Greene, 2003a,b), the expression for R remains the same but r_i is taken to be the distance between atoms j and k and the coordinates are given by

$$r_1 = 3^{-1/4} R \sqrt{1 + \sin\theta \sin\left(\phi + \frac{2\pi}{3}\right)}, \tag{15}$$

$$r_2 = 3^{-1/4} R \sqrt{1 + \sin\theta \sin\left(\phi - \frac{2\pi}{3}\right)}, \tag{16}$$

and

$$r_3 = 3^{-1/4} R \sqrt{1 + \sin\theta \sin\phi}. \tag{17}$$

From Equations (15)–(17) one can derive expressions for θ and ϕ, which become intuitively meaningful by consulting Figure 6 in the work of Kokoouline and Greene (2003a) for a valuable demonstration of the meanings of these angles. [For further discussion of hyperspherical coordinates, the reader is referred to the review by Lin (1995)]. The general idea is that the hyperradius describes the overall size of the molecule, whereas the hyperangles, which are not explicitly defined in the first paper, describe the shape of the molecule. These considerations lead to the adiabatic hyperspherical approximation in which motion in R is considered to be much slower than the motion in the hyperangles, i.e., as the atoms traverse the potential surface, the shape of H_3^+ changes more rapidly than the overall size of the molecule. With the motion in the hyperangles separated from the motion in R, a Schrödinger equation at a single value of R can be written in which the eigenvalue is a point on the potential curve. The hyperradius, R, is identified as the polyatomic analog to the familiar diatomic internuclear distance. But is this analogy appropriate? The familiar Born–Oppenheimer approximation is an adiabatic treatment of the nuclear motion and is justified by the great difference in the electron and nuclear masses. However, in the adiabatic hyperspherical approach for H_3^+, the particles are all of equal mass. This approach is tested (Kokoouline & Greene, 2003a and 2003b) by solving for the nuclear vibrational energies within the generated potential curves. The eigenvalues for several low-lying levels differ by less than $23\,\mathrm{cm}^{-1}$ from a full three-dimensional

diagonalization (Jaquet et al., 1998), and the results support the use of this approximation. In later work (Fonseca dos Santos et al., 2007), this approximation is partially dropped (see below).

While the adiabatic hyperspherical approximation for H_3^+ appears to be successful for the vibrational energies, there have been no reported tests of the accuracy of the amplitudes of the vibrational wave functions. Inaccuracies in the amplitudes may significantly affect the values of important matrix elements between Rydberg states. It is interesting to note that the adiabatic hyperspherical approach fails for H_2D^+ and D_2H^+ (Kokoouline & Greene, 2005).

4.5.2 Potential Surfaces and Jahn–Teller Coupling

The potential surface of H_3^+ used by Kokoouline et al. (2003) is from Cencek et al. (1998) and Jaquet et al. (1998), and the H_3 surfaces are from the work of Siegbahn and Liu (1978), Truhlar and Horowitz (1978), and Varandas et al. (1987). These surfaces need to be interpolated to be converted to a grid in hyperspherical coordinates, but this is not covered in the published papers.

The main driving force for DR, introduced for the first time in these calculations, is the JT coupling (Jahn & Teller, 1937), a coupling which does not occur in diatomic molecules. Figure 6 shows that the two lowest states of H_3 intersect. The intersection point is at the equilateral triangle configuration where the molecule has D_{3h} symmetry. The two lowest states have two electrons distributed in the three H 1s orbitals and one electron that is either in a $2p_x$ or $2p_y$ orbital where the molecule is in the *xy* plane. As R_2 (see Figure 5) moves away from the equilateral triangle value (1.43 a_0) but with Θ fixed at 90°, the molecular symmetry is lowered to C_{2v} and the degeneracy is split. The splitting is known as the static JT effect. The degeneracy at the D_{3h} configuration appears as a point of conical intersection when the potential surfaces are plotted in normal coordinate space, not Cartesian coordinate space. A further splitting of the energies of the original vibrational levels (in the wells of the $2p_x$ or $2p_y$ electronic states) occurs when the levels are determined in the mixed state. This splitting arises from the dynamic JT effect. An excellent description of the JT effects can be found in the work of Herzberg (1966).

For H_3 (Greene et al., 2003), the JT mixing has used the *K*-matrix form of Staib and Domcke (1990) and the JT mixing parameter and quantum defects, μ, of Mistrík et al. (2000), which was obtained from a fit to *ab initio* surfaces. The nature of the conical intersection allows one to represent the coupling with two parameters [see Equation (4.7) of Mistrík et al. (2000)]. This is an enormous simplification compared to other situations where a non-JT coupling may need to be represented by a surface of derivative couplings. Of further importance, Staib and Domcke (1990) reported that

the fit to the *ab initio* results of Nager and Jungen (1982) shows that the conical shape of the potential surfaces is close to a true cone, although data to support this observation were not reported. This observation means that higher JT interaction terms beyond linear may not be needed and that the interaction of the np series with the ns or nd series is not important since if they were important a distorted conical shape would occur. Here, n is the principal quantum number. These observations provide some justification for the use of only an $\ell = 1$ partial wave for the incoming electron in the calculations of Kokoouline and Greene (2003). On the other hand, Mistrík et al. (2000, 2001) found evidence for strong mixing of the ns and nd Rydberg states with 3p, 4p, and 5p states built on H_3^+ cores having the degenerate asymmetric vibrational motion. A point on the 5pE′ surface was found to have only 80% p character.

The JT coupling parameter and the quantum defects used (Kokoouline et al., 2003a, b) are for the 4pπ state of H_3 (Mistrík et al., 2000). Ideally, the best coupling parameters and the best quantum defects would vary with the Rydberg or continuum orbital energy. However, these are not available. In addition, for $n \geq 3$ the quantum defect varies only slightly with n but that for $n = 2$ differs considerably from those for $n \geq 3$. Because the MQDT approach requires a single coupling parameter and a single quantum defect surface, one must choose a compromise value. Usage of the $n = 4$ quantum defects (Kokoouline et al., 2003) should produce only very small errors in the positions of resonances, but the $n = 2$ states will suffer the largest shift in energy from the true positions.

The JT interaction is generally thought of as that between states having the same n^*. Here n^* is the effective principal quantum number, i.e., $n^* = n - \mu$, and μ is the quantum defect. In the MQDT approach used by Greene and coworkers, the JT interaction not only describes the interaction between the two E′ states having outer orbitals $2p_x$ and $2p_y$ but also accounts for the mixing of Rydberg states with different n^*, the mixing of Rydberg states with continuum states, and the mixing of the Rydberg and continuum states with the 2pE′ dissociative states. This assumes that these mixings are symmetry allowed. Rydberg orbitals of differing n^*, although orthogonal to each other, are quite similar near the nuclei except for a normalization factor of $1/n^{*3/2}$. Since it is the Rydberg amplitude near the nuclei that is most important, the JT effect will occur between Rydberg states and the two dissociative states, scaled by the $1/n^{*3}$ factor. The normalization constant is squared since the width [see the expression below Equation (14)] has the square of the interaction matrix element. If the incoming electron is in a p_x continuum orbital, it can be captured into an np_y orbital also scaled by the $1/n^{*3}$ factor. For two different Rydberg states having effective principal quantum numbers of n_1^* and n_2^*, the connecting width would scale as $1/(n_1^* n_2^*)^3$.

The couplings mix the Rydberg and continuum states with the lowest $n = 2$ dissociative states along which DR is finalized.

The mixing of all the Rydberg states with each other and that of the continuum state with all the Rydberg states means that many possibilities for DR can occur. The continuum electron can be directly captured into the $2p_{x,y}$ states followed by dissociation, or it can be captured into a higher state which, via couplings to other intermediate levels, can eventually lead to the dissociative levels. The mechanism is remarkably similar to one originally proposed by Bates et al. (1993).

4.5.3 Nuclear Spin

The nuclear spin has been included in prior theoretical studies of homonuclear diatomic DR whenever molecular rotation is considered. The calculations reported by Greene and coworkers also include nuclear spin in the theory. Nuclear spin cannot be ignored because in H_3, the nuclei are fermions and the total wave function must change sign for an interchange of any two protons. (The exchange is equivalent to a rotation by 180° around an axis perpendicular to the main symmetry axis.) This requirement places restrictions upon the allowed values for the rotational quantum numbers and requires that the total symmetry (i.e., the product of the symmetries of the vibrational, rotational, nuclear spin and electronic wave functions) be that of the A_2' or A_2'' representations of D_{3h}. The ortho and para states have total nuclear spin of 3/2 and 1/2, respectively.

4.5.4 Calculation of the DR Cross Section and Rate Coefficient

The first paper (Kokoouline et al., 2001) reported preliminary calculations which made use of the hyperspherical adiabatic approach and an expression derived by O'Malley (1966) for the direct DR cross section, σ, of diatomic molecules:

$$\sigma = \sum_{\beta} \frac{\pi^2}{E_{\mathrm{el}}} \frac{\Gamma_\beta R_\beta}{\left|U'_\beta R_\beta\right|} \left|\Psi R_\beta\right|^2 \tag{18}$$

In Equation (18) β is an index that runs over the dissociative routes, E_{el} is the electron energy, R_β is the value of the hyperradius for the β^{th} dissociative route at an energy, E_{el}, above the ion rovibrational level undergoing DR, Γ_β is the width for capture into the β^{th} dissociative route, U_β' is the slope of the β^{th} dissociative route, and $\Psi(R_\beta)$ is the dissociative nuclear wave function. The use of this expression follows from the observation that when the potential curves are plotted as a function of the hyperradius, all the Rydberg states cross the ion ground state.

Equation (18) omits the survival factor [the denominator within parentheses in Equation (14)] and thereby does not account for autoionization. There are several other caveats to consider. This expression was derived for diatomic molecules and its use for H_3^+ entails replacing the internuclear distance by the hyperradius. This replacement is not likely to lead to quantitative results. In diatomics, the nuclear configuration depends solely upon the internuclear distance, and the Franck–Condon factor in Γ_β has a rigorous dependence upon this distance. In a triatomic, in hyperspherical coordinates, the Franck–Condon factors will depend upon both the hyperradius and the hyperangles. Since the hyperradius is often viewed as a measure of the size of the molecule, taking Γ_β to depend only upon R_β is making the approximation that the Franck–Condon factors depend more upon molecular size than upon the details of molecular shape. This approximation is not expected to be reliable. It is probably for these reasons that the results (Kokoouline et al., 2001) are referred to as preliminary and approximate. Both upper and lower bound cross sections were reported. The lower bound cross sections included only the 2p states. Both the 2p and higher np states are included in the upper bound cross section. In a later paper (Kokoouline & Greene, 2003b), it is noted that the cross sections reported in the first paper (Kokoouline et al., 2001) need to be multiplied by a factor of π^2 due to inconsistencies in the literature concerning the definition of the K matrix. Surprisingly, if one multiplies the 2001 results by π^2, the upper bound cross section is in quite good agreement with the storage ring results (Jensen et al., 2001). The calculated cross sections are structureless as are the experimental results to which they were compared. Using only the 2p states, it is estimated that 70% of the DR events lead to $H + H + H$ compared to the experimental result (Datz et al., 1995a, b) of $75\% \pm 8\%$. For the $H + H_2$ channel, the peak H_2 vibrational distribution occurs at $v = 5$–6 compared to the broad distribution found experimentally, which peaks at $v = 5$ (Strasser et al., 2001). The upper bound thermal rate coefficient at 300 K is 1.2×10^{-7}cm^3/s after correction by the π^2 factor and compares well to the storage ring results of 1.0×10^{-7}cm^3/s (Jensen et al., 2001) and 1.15×10^{-7}cm^3/s (Sundström et al., 1994). The usage of Equation (18) to calculate these results would lead one to conclude that this agreement must be fortuitous. However, the agreement reported not only for the cross section and rate constant but also for the branching fraction and vibrational distribution argues otherwise.

4.5.5 Improved Cross Sections

The lack of structure in the calculated cross section was corrected in a later detailed paper (Kokoouline & Greene, 2003b), which used an MQDT approach instead of Equation (18). The use of the adiabatic

hyperspherical approximation has been described above as has the K matrix having the JT coupling.

The calculated rate coefficients are reported (Kokoouline & Greene, 2003a and 2003b) to be accurate to better than 20% due to the incomplete set of states that are included in the calculations. The states are characterized by the quantum numbers [I, Γ, N^+, N], where I represents the two values for the total nuclear spin, 3/2 (ortho) and 1/2 (para), Γ denotes the total molecular symmetry ($A_2^{'}$ or $A_2^{''}$), and N^+ and N denote the rotational quantum number for H_3^+ and H_3, respectively. (The total molecular symmetry is determined by the need to have the total wave function change sign upon a swap of any two nuclei.) In the first detailed report of the calculations (Kokoouline & Greene, 2003b), 17 sets of these quantum numbers were used, each with 8–12 vibrational wave functions (including the continuum) and 50–100 hyperspherical potential curves. A tabulation of the levels is not included.

In the most recently reported calculations (Fonseca dos Santos et al., 2007), several improvements were incorporated into the cross section and rate constant calculations. The adiabatic hyperspherical approximation was relaxed by including couplings between the adiabatic channels. The slow variable discretization approach was used to incorporate these couplings, but the details of these new calculations are not reported. A comparison of the calculated vibrational energies for 26 low-lying vibrational states with a full three-dimensional diagonalization (Jaquet et al., 1998) shows a clear improvement over the earlier full adiabatic approach (Kokoouline & Greene, 2003b). The positions of the Rydberg resonances are improved with this revision.

However, the physical interpretability of these calculations is somewhat problematic. Potential curves plotted as a function of the hyperradius are much more difficult to interpret than the more familiar surfaces plotted as a function of Cartesian coordinates. Furthermore, if one improves upon the adiabatic hyperspherical approach by including more couplings between the curves, the concept of a potential curve as a function of the hyperradius becomes weak. In the limit of completely dropping the adiabatic hyperspherical approximation, potential curves are no longer meaningful. These considerations must be balanced against the reasonable agreement that has been obtained to date between these calculations and experiment. This is discussed further below.

An important additional improvement in the most recent calculations (Fonseca dos Santos et al., 2007) is the addition of more resonance states. Rotational states up to $N^+ = 5$ are included compared to the prior calculations which included levels up to $N^+ = 3$ (but not $K^+ = 1$) and (4, 3) for the ground vibrational level. A detailed accounting of the included vibrational levels is not presented, which makes it difficult to assess whether or not the theoretical treatment is adequate at particular electron energies.

4.5.6 Toroidal Correction

In the storage ring experiments, a beam of molecular ions circulates in a large ring (51.6-m circumference) (Strömholm et al., 1996) and merges with a beam of electrons in only a small section (0.85 m) (Strömholm et al. 1996) of the ring known as the electron cooler (the region between the merging and demerging regions in Figure 3). The electron beam is bent by a toroidal magnetic coil at the beginning and end of the overlap region. Collisions between the continuously renewed electron beam and the ions serve to reduce the random motions of the ions leading to a high energy resolution. The ion beam is generally a few mm in diameter compared to the electron beam which is a few cm in diameter.

The cooler is also the location where DR takes place. For measurements at "zero" center of mass energy, the electron beam is velocity matched with the ion beam. For other center of mass energies, the electron beam energy is shifted up or down from the "zero" energy measurement. For most of the length of the cooler, the electron beam is very closely collinear with the ion beam and the intended center of mass energy is appropriate. However, in the merging and separating regions at both ends of the cooler, the ion and electron beams are not parallel and the center of mass energy changes with the angle between the two beams. The result is that a measurement of the DR rate constant at a single center of mass energy (appropriate in the straight section of the electron beam cooler) is actually an average of rate constants for different center of mass energies over the length of the cooler from the beginning of the merging region to the end of the separating region. The bending region comprises only about 15% (Amitay et al., 1996) of the full length of the overlap of electron and ion beams and was thought to not play a significant role in deriving the value of the rate constants. However, an important recent study by Kokoouline and Greene (2005) on H_3^+ indicates that the experimental data deviate considerably from the theoretical values near 0.03 eV, 0.1 eV, and above 0.8 eV. In the latter region the difference between experiment and theory is over an order of magnitude. If the theoretical results are averaged over the full cooler length, accounting for the higher relative center of mass energies at the ends of the cooler, the theory agrees with experiment above 0.8 eV and shows improved agreement at 0.03 and 0.1 eV. The results indicate that raw storage ring data must be corrected to remove the effect of the electron bending regions. The deconvolution procedure for accomplishing the correction (Lampert et al., 1996) introduces considerable uncertainty because the rate constants needed at higher energies have often not been measured, and in the case of those that have been measured, they too must be corrected. The result is an iterative procedure which is usually carried out to first order (i.e., a single iteration) (Strömholm et al., 1996).

4.5.7 Breit–Wigner Cross Sections

If one assumes that all electron captures into Rydberg states lead to dissociation in one way or another and that there is no direct dissociative channel that would interfere with the dissociation through the Rydberg states (as is the case for H_3), the Breit–Wigner expression can be used for calculating DR cross sections. An important innovative approach along these lines has been reported by Jungen and Pratt (2009). They treated the linear JT effect, restricting capture into $v_2 = 1$ Rydberg levels (from the ion ground state). Capture into $v_1 = 1$ Rydberg levels was not considered. Using spectroscopic data for the 3pE′ state and previously determined JT coupling parameters, they show that after averaging over the closely spaced $v_2 = 1$ resonances, a simple cross section expression results which is independent of n^* and structureless.

4.5.8 Comparison of Theory and Experiment

For the four isotopomers, Jungen and Pratt (2009) show that there is a factor of two disagreement with the experimental rate coefficient at some energies for D_3^+ and a factor of 2–3 disagreement for D_2H^+. For H_2D^+ and H_3^+ the agreement is even better except near 0.006 eV for H_3^+. The resulting rate coefficients show remarkable agreement with experimental results for the four isotopomers considering the simplicity of the cross section expression. Figure 14 has the latest results of Greene and coworkers (Fonseca dos Santos et al., 2007), Jungen and Pratt (2009), and the CRYRING (McCall, 2004) data for H_3^+. The theoretical results of Fonseca dos Santos et al. (2007) show much more structure than the CRYRING data. Although the theory and experiment are in generally good agreement, there is clearly room for improvement.

4.5.9 Suggestions for Future Theory

The pioneering research of Greene, Kokoouline, and coworkers has made an enormous contribution to our understanding of the DR of H_3^+. Nevertheless, many of the details remain to be uncovered. We still do not know which Rydberg states drive DR. The identities of the important states will change with electron energy as will the details of the mechanism. An important contribution in this regard has been the theoretical work of Tashiro and Kato (2002, 2003) on the predissociation lifetimes of H_3 Rydberg states. They found that the $2s^2A_1'$ state has a large coupling with the upper 2pE′ state (see Section 4.4.4) and may be a feeder state for DR from higher Rydberg states. They propose that in DR, initial electron capture occurs into high n ($n = 6$ or 7) states with low vibrational excitation followed by coupling to lower n states with higher vibrational

excitation. The coupling eventually leads to the $2s^2A_1'$ state, which is predissociated mostly by the upper 2pE′ state. They propose that if electron capture involving a single vibrational quantum is most important, the $6s^2A_1'(1, 0^0)$ and $7p^2E'(0, 1^1)$ are important for DR at electron energies just above the lowest vibrational level of H_3^+. By propagating a wave packet from $7pE'(0, 1^1)$, they find that the predissociation involves the intermediate states $5p^2E'$, $4s^2A_1'$, $3s^2A_1'$, $3p^2E'$, $2s^2A_1'$, and finally DR via 2pE′. However, the precise identification of these states requires greater accuracy in the quantum chemical determinations of their positions and widths and would be a valuable contribution. Note that the $2s^2A_1'$ state and those for $n > 2$ are not included in the calculations of Greene, Kokoouline, and coworkers or those of Jungen and Pratt (2009) and should be considered for future work.

Future theoretical studies should explore the role of the $\ell = 0$ and 2 partial waves. The work of Tashiro and Kato (2002) indicates that the $\ell = 0$ wave may be more important than $\ell = 2$. The calculations of Greene, Kokoouline, and coworkers and Jungen and Pratt (2009) treated only $\ell = 1$. The inclusion of the $\ell = 0$, 2 partial waves may account for some of the differences between theory and experiment.

The JT coupling explored by Greene and coworkers is probably the dominant coupling that drives DR. But other derivative couplings that have been identified in prior calculations (Schneider & Orel, 1999; Schneider et al., 2000; Tashiro & Kato, 2002) need to be included in future three-dimensional calculations.

The failure of the adiabatic hyperspherical approach for H_2D^+ and D_2H^+ leads one to ask if it is entirely adequate for H_3^+. Instead of calculating vibrational energies to determine the accuracy of this approach, it may be more meaningful to compare the values of S matrix elements resulting from the adiabatic hyperspherical approach to elements calculated by relaxing this approach.

5. HISTORY OF EXPERIMENTAL H_3^+ RECOMBINATION STUDIES

As may be seen in Figure 10, the measured recombination coefficients have varied considerably over the years. While all afterglow measurements carried out before 1973 probably refer to mixtures of H_3^+ and H_5^+ ions (and impurity ions), the recombining H_3^+ ions were clearly identified by mass analysis in the microwave afterglow studies by Leu et al. (1973). The measured recombination rates were very similar to those found for many other ions and nothing unusual was noted. Subsequent studies used either an inclined-beam (Peart & Dolder, 1974) or single-pass merged-beam (Auerbach et al., 1977) measured recombination cross

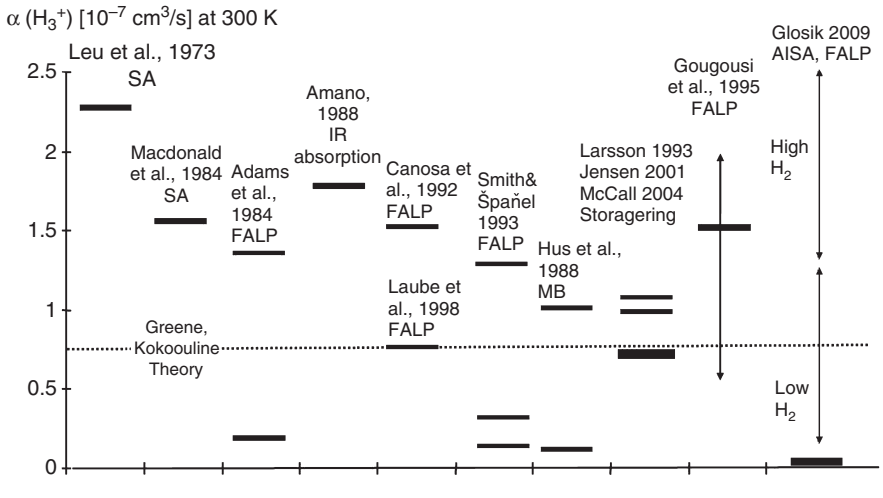

Figure 10 H_3^+ recombination coefficients inferred from different types of experiments, at electron temperatures near 300 K

sections over a wider range of energies, confirming the afterglow data within about a factor of two. Macdonald et al. (1984) extended the microwave measurements to higher electron temperatures up to 5000 K by microwave heating of the plasma electrons. While the measured 300 K rate coefficients were somewhat smaller than those of Leu et al. (1973), the temperature dependence was quite close to that expected from the merged-beam results.

Not much attention was paid at that time to a theoretical argument by Kulander and Guest (1979) that the usual curve-crossing DR mechanism would not be applicable in the case of H_3^+. The situation changed when Michels and Hobbs (1984) again calculated one-dimensional potential-energy curves of H_3^+ and showed that the ionic ground-state curve of H_3^+ in the lowest vibrational states does not intersect a repulsive curve leading to neutral products. However, suitable curve crossings, were found for H_3^+ ions in the third or higher vibrational states. Hence, Michels and Hobbs suggested that the experimental data referred to vibrationally excited H_3^+ ions. Their argument was seemingly strengthened by new experimental data of Adams et al. (1984), who used their new "Flowing Afterglow Langmuir Probe" (FALP) technique to study the recombination of H_3^+. They noticed that the initial electron-density decay was quite fast, compatible with a recombination coefficient near 10^{-7} cm^3/s, but also that it changed in the later afterglow to a slower decay indicating a much smaller ($<2 \times 10^{-8}$ cm^3/s) recombination rate coefficient. Michels' and Hobbs' prediction offered a ready explanation for this

observation, namely that the initial fast decay was due to recombination of vibrationally excited ions ($v \geq 3$) and that the slow decay should be ascribed to H_3^+ in $v = 0$. Later, Adams and Smith reported that the recombination rate for $v = 0$ ions might be even smaller ($\sim 10^{-11}$ cm^3/s). Larsson and Orel (2008) provide a brief account of these experiments, which were not published in detail. While this very low value may have been due to an experimental problem (presence of nonrecombining He^+ ions) it became generally (with some exceptions) accepted that H_3^+ in the vibrational ground-state recombined only slowly.

The interpretation of Adams et al. experiment became highly questionable when Amano (1988, 1990) used infrared absorption to monitor the decay of the H_3^+ ($v = 0$) density in the afterglow of a radio-frequency discharge in pure hydrogen. At a gas temperature of $T = 210$ K Amano measured a recombination coefficient for $v = 0$ ions of 1.8×10^{-7} cm^3/s, fairly close to the data of Leu et al. and Macdonald et al. The ensuing debate at times became rather contentious. Responding to some criticism, Smith and Špaňel (1993) repeated the original studies by Adams et al. (1984) in much greater detail and arrived at the conclusion that $v = 0$ ions recombined with $\alpha = (3.6 \pm 1) \times 10^{-7}$ cm^3/s, somewhat faster than their previous result.

The measurements by Amano suggested that curve crossing might not be as essential for recombination as had been thought. Bates et al. (1993), in a paper entitled "Enigma of H_3^+ dissociative recombination," proposed a multistep mechanism to rationalize experimental results, but the theory was not sufficiently quantitative to dispose of the "enigma."

Additional flowing-afterglow measurements were carried in attempts to settle the question. One study (Canosa et al., 1992) gave rate coefficients of 1.1×10^{-7} cm^3/s at $T = 650$ K for H_3^+, thought to be in $v = 0$, and 1.5×10^{-7} cm^3/s at 300 K for ions believed to be of low vibrational excitation ($v \leq 2$). A further study in the same laboratory by Laubé et al. (1998) resulted in a factor-of-two lower value of 7.8×10^{-8} cm^3/s at 300 K. This value is often quoted as the afterglow measurement that agrees best with the storage ring results. However, the authors also carried out an identical experiment for D_3^+ and found essentially the same recombination coefficient as for H_3^+, and this does not agree with the storage ring data.

Gougousi et al. (1995), using the flowing afterglow techniques, observed a decline of the recombination rate at late times and found that the apparent recombination rate (inferred from the early afterglow decay) increased from 1.5×10^{-7} cm^3/s to nearly 2×10^{-7} cm^3/s when the experimental H_2 concentration was raised from 1×10^{14} cm^{-3} to 15×10^{14} cm^{-3}. They attempted to explain their data by a model in which H_3^+ recombination occurred by a three-body mechanism in which both electrons and neutral hydrogen play a role.

Later studies using the single-pass merged-beam method did not lead to consistent results. For instance, Hus et al. (1988) found a nearly

20 times larger cross DR cross section when the "rf source" was used rather than the "trap source" to produce ions. In single-pass measurements, the ions do not have sufficient time to relax vibrationally or rotationally before merging with the electron beam, and hence it seemed possible that the observed effects were due to vibrational excitation of the ions, as was suggested by the authors. Mitchell [unpublished, brief accounts are contained in a paper by Johnsen and Mitchell (1998) and by Mitchell and Rogelstad (1996)] also carried out a merged-beam experiment in which the deflection field used to separate product neutrals from the ions in the post-collision region was varied. The measured DR product signal increased by a factor of 5 (approaching that obtained in storage-ring experiments) when the field strength in that region was reduced from 3000 V/cm to 200 V/cm. Mitchell ascribed this effect to field ionization of H_3 Rydberg molecules that are produced by DR of H_3^+. At the high field strength, but not at the lower, a substantial fraction of the recombination H_3 Rydberg products would be re-ionized in the demerging region of the apparatus and would not be counted as DR products. The problem with this suggestion is that it does not really remove the discrepancy between the merged-beam and storage ring data since field ionization should also occur in the bending magnet of storage ring experiments. A convincing explanation of these observations has not yet been given.

Since then, afterglow measurements on H_3^+ and D_3^+ have been carried out almost exclusively by Glosík and coworkers in Prague, who use both a flow tube and an advanced stationary afterglow apparatus (AISA). The Prague group systematically studied the dependence of the apparent rate coefficients as a function of gas densities and temperature. A nearly complete set of their data has been presented in a recent paper (Glosik et al., 2009a).

The Prague group (Macko et al., 2004) also carried out a series of afterglow measurements in which the $H_3^+(v=0)$ ion density during the afterglow was measured by optical absorption using a cavity ring-down technique. These results confirmed the spectroscopic measurements by Amano (1988 and 1990) and show that vibrationally cold ions recombine with coefficient of about $\sim 1.5 \times 10^{-7}$ cm^3/s.

The most interesting and startling observations made by the Prague group (see, e.g., Plašil et al., 2002) were that the DR rate coefficients seem to fall off rapidly (down to $\sim 1 \times 10^{-9}$ cm^3/s) when the H_2 concentration is reduced to below 10^{12} cm^{-3}. It is this observation that challenges the now generally accepted rate coefficient of $\sim 1 \times 10^{-7}$ cm^3/s and seemingly poses a serious problem. We will show later (see Section 6.1) that those afterglow data do not really support the very low inferred recombination rates.

The modern era of DR studies of H_3^+ and D_3^+ (and many other ion species) began with the extensive work using ion-storage rings, the CRYRING in Stockholm, the ASTRID ring in Aarhus, and the TSR in

Heidelberg. Unlike the afterglow and single-pass merged-beam work, this technique produced remarkably consistent results. Steady improvements in the energy resolution, control and characterization of vibrational and rotational states, and beam quality were made over the years, but the conclusions never changed significantly. The latest results of the CRYRING and TSR rings show a nearly identical dependence of the rate coefficient (or cross section) on energy, including the finer structures that will be discussed later. The thermally averaged (Maxwellian) rate coefficient as a function of electron temperature, derived from the CRYRING results (McCall et al., 2004), can be expressed by an analytical fit of the form

$$a(T_e)[\mathrm{cm}^3/\mathrm{s}] = -1.3\times10^{-8} + 1.27\times10^{-6}T_e^{-0.48}, \tag{19}$$

which gives a recombination coefficient of 6.9×10^{-8} cm^3/s at $T_e = 300$ K. This value refers to ions in the lowest vibrational state, and at a rotational temperature of about 30 K.

6. RECONCILING AFTERGLOW AND STORAGE RING RESULTS

The history of afterglow measurements of H_3^+ recombination rates presents a rather confusing picture. If one accepts the agreeing storage ring and theoretical value of $\alpha(300\,\mathrm{K}) = 7\times10^{-8}$ cm^3/s as a "benchmark," then some afterglow measurements yielded values that were "too small" by factors of 10 and more, while others are "too large" by factors of 2–3. The question then arises which of the afterglow observations reflect a real difference in recombination mechanisms and which ones are due to experimental errors.

6.1 Afterglow Measurements That Yielded Very Low Recombination Coefficients

We will discuss the unusually low values first. There are good reasons to believe that plasma recombination can be enhanced by third-body-assisted recombination, but it is difficult to envision a mechanism that suppresses binary H_3^+ recombination in the plasma environment. One might surmise that the H_3^+ ions in the experimental plasmas were of a particular type, for instance in a nonrecombining vibrational state or perhaps in different spin modification, e.g., ortho or para H_3^+. At this time, it appears very unlikely that vibrationally excited H_3^+ ions recombine more slowly than those in the ground state, as was suggested in a previous review by one of the present authors (Johnsen, 2005).

New theoretical calculations by Fonseca Dos Santos et al. (2007) for the E (0, 1^1)] and A_1 (1, 0^0)] vibrationally excited states actually indicate the opposite so that this "loop hole" has essentially been closed. Likewise, recent storage ring experiments (Tom et al., 2009) and theory (Fonseca dos Santos et al., 2007) indicate that both the ortho and para spin modifications of H_3^+ recombine at nearly the same rate, at least at 300 K. The storage ring results show that the ortho form recombines somewhat more slowly, but only by about a factor of 1.5.

The most puzzling findings that need to be examined in some detail are those made in the extensive series of stationary- and flowing-afterglow measurements by the Prague group (Glosik et al., 2009a; Plašil et al., 2002). Their experiments seemed to indicate that the H_3^+ recombination rate dropped to values far below the binary value (by a factor of 10 and more) when the hydrogen concentration in the experiments was reduced from about 1×10^{12} cm^{-3} to 1×10^{11} cm^{-3}. Very similar results were consistently obtained by the two different afterglow methods, at different temperatures, and also for D_3^+ ions (Glosik et al., 2009b). This finding is often mentioned as a serious problem since it is in conflict with both recent theory and experiments.

It is always difficult to reanalyze experimental data that were taken by others. However, if one examines the experimental conditions, one realizes that the expected recombination rate of about 10^{-7} cm^3/s could not have been observed at low H_2 concentrations. While the two reactions in the sequence $Ar^+ + H_2 \rightarrow ArH^+ + H$ and $ArH^+ + H_2 \rightarrow Ar + H_3^+$ are fast (rate coefficients near 10^{-9} cm^3/s), it will still take roughly 10 ms at $[H_2] = 10^{11}$ cm^{-3} to produce H_3^+ ions, but recombination of an ion with $\alpha = 10^{-7}$ cm^3/s (at $n_e = 10^{10}$ cm^{-3}) proceeds at a time scale of $1/(\alpha n_e) = 1$ ms. This means that the loss rate of electrons in the plasma is not limited by recombination, but by the rate at which the ion is formed. Since our criticism affects a large set of published data, we constructed a simple numerical model that simulates the afterglow processes and the methods of analysis that were employed by the Prague group. The authors determine recombination coefficients using a form of data analysis in which one constructs a graph of the measured values of the quantity

$$-\left(\frac{1}{n_e^2}\frac{dn_e}{dt} + \frac{\nu_D}{n_e}\right) \tag{20}$$

as a function of the reciprocal electron density. Here ν_D describes the loss of ions and electrons due to diffusion in the fundamental diffusion mode. If the plasma contains only one recombining ion species from the very beginning, or if this condition is approached rapidly, then a graph of this kind indeed approaches the value of the recombination coefficient in the limit of $n_e \rightarrow 0$ (i.e., the late afterglow). In practice, the asymptotic

value is attained in a short time if the reactions forming H_3^+ go to completion rapidly, which is the case in most afterglow measurements when the H_2 density is sufficiently high. However, this is not true when the H_2 density is very low.

Our numerical model returns the values in the expression above as a function of the reciprocal electron density. To keep the model simple, we ignore depletion of the neutral H_2 due to the ion–molecule reactions, even though it is not negligible, but including it would make the situation only worse. The model shows that an input value of $\alpha = 10^{-7}$ cm^3/s and initial electron densities of 1×10^{10} cm^{-3} leads to same inferred recombination coefficient only if $[H_2] > 10^{12}$ cm^{-3}. At $[H_2] = 1 \times 10^{11}$ cm^{-3} (see Figure 11) graphs of the same kind show that the asymptotic value is never approached on the time scale of the experiment (about 40 ms). The authors' method of recovering the recombination coefficients employed a linear extrapolation (sometimes done approximately on a logarithmic graph) toward $1/n_e \to 0$. The procedure returns a much smaller and incorrect value of the recombination coefficient. The asymptotic value approached in the limit $n_e \to 0$ should have been used, but in practice this value cannot be obtained at low $[H_2]$, even by curve-fitting, with any reasonable degree of precision, since diffusion becomes the dominant loss in the late afterglow. Another way of illustrating the cause of the problem is to examine the evolution of the ion composition during the afterglow, an example of which

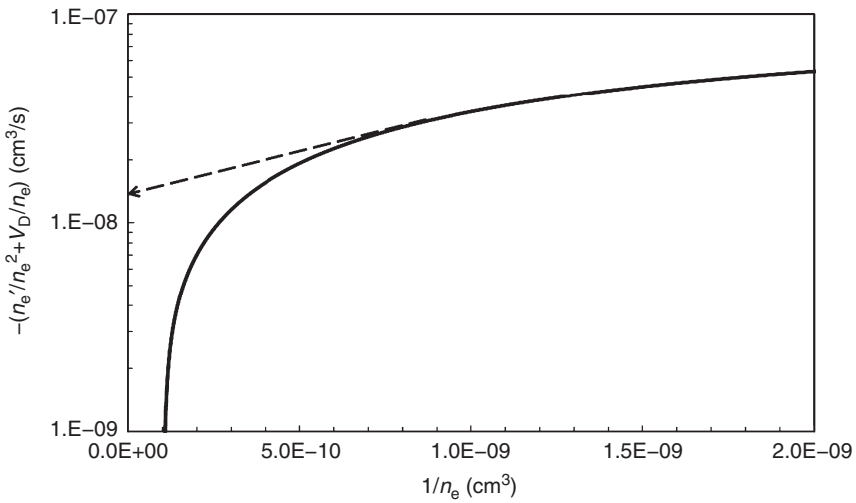

Figure 11 Numerical simulation of an afterglow in an helium/argon/hydrogen mixture at a hydrogen concentration of 1×10^{11} cm^{-3} for an assumed H_3^+ recombination coefficient of 1×10^{-7} cm^3/s. The arrow indicates the extrapolation to $1/n_e = 0$, from which a far smaller recombination coefficient is obtained

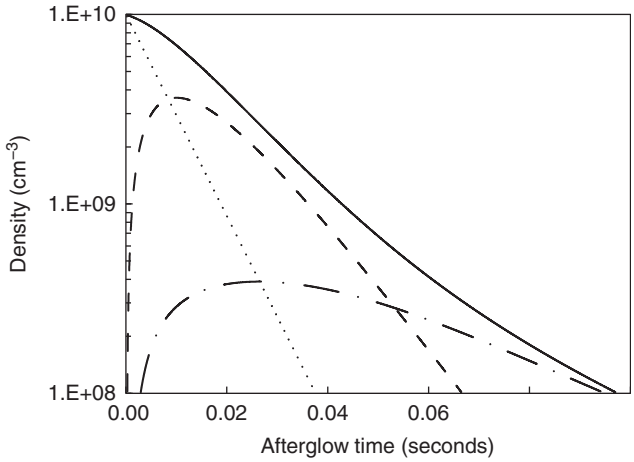

Figure 12 Numerical simulation of an afterglow in a helium/argon/hydrogen mixture at a hydrogen concentration of 1×10^{11} cm^{-3} for an assumed H_3^+ recombination coefficient of 1×10^{-7} cm^3/s. The lines indicate the evolution of density of electrons (thick line), Ar^+ ions (dotted line), ArH^+ ions (dashed line), and H_3^+ ions (dash-dotted line)

is given in Figure 12. Even at an afterglow time of 40 ms, H_3^+ accounts for only 1/3 of all ions, which makes it impossible to obtain accurate H_3^+ recombination coefficients. The authors did carry out simultaneous mass spectrometric observations that seemed to indicate that the plasma was dominated by H_3^+ ions. However, the mass spectrometer samples ions from a region near the wall of the plasma container where the electron density and recombination loss of H_3^+ is lower, and hence the relative abundance of this ion is higher than it is in the center of the plasma.

We conclude that the observations of very low recombination rates at low [H_2] are probably in error and that consequently there is no need to search for explanations in terms of H_3^+ recombination mechanisms. In reality, the situation may be more complicated. A slower increase of the recombination coefficient with H_2 concentration is consistently observed at much higher [H_2] and this effect must have a different origin (see Section 6.3). While attempting to fit some of the published data samples, we also noticed that better fits were obtained when the model H_2 concentration was reduced to values below the stated concentrations. This may indicate that a fraction of the H_2 was dissociated during the discharge phase of the experiment in the stationary afterglow experiments. Some dissociation of H_2 can also occur in flowing afterglow measurements due to metastable argon atoms that enter the recombination region. These remarks are speculative. It may be worthwhile to conduct some experiments to clear up such questions.

A further observation of very low recombination rates was made by Adams et al. (1984) in an afterglow experiment. This observation had a great impact and for a while since it was believed to provide evidence that H_3^+ ions in their vibrational ground state recombined only slowly. Their experiments showed that the electron density in an H_3^+ afterglow initially decayed quite fast (indicating a recombination rate of about 1.3×10^{-7} cm^3/s) but then decayed much more slowly. No such effects were found when the plasma contained O_2^+ ions. At the time when the experiments were done, it was believed that H_3^+ in the vibrational ground state recombined very slowly. Hence the experimenters drew the natural conclusion that the initial decay was due to vibrationally excited H_3^+ and that the later slower decay was due to ground state ions. The lowest 300 K recombination coefficient derived in a later repetition of this experiment by Smith and Špaňel (1993) was 3×10^{-8} cm^3/s, lower by a factor of 2.3 than the storage ring value. The authors believed that this value referred to a mixture of $v = 0$ and $v = 1$ ions. However, the accuracy of this value must be regarded as questionable. It was obtained by fitting the observed decay to a model that has too many adjustable parameters, the relative abundance of the two (or possibly three) states, two recombination coefficients, the quenching coefficient from the higher to the lower state, an estimated impurity concentration, and a diffusion rate. Also, the deviation of the decay curve from that corresponding to a simple (single-ion) decay is actually very small (only a few %), which makes it difficult to determine several coefficients by curve-fitting. While a good fit to the data was obtained, it does not necessarily result in a unique value of the recombination coefficient in the late afterglow. We constructed a simple numerical model similar to the one used by the authors and found that equally good fits could be obtained for higher recombination rate coefficients (up to about 6×10^{-8} cm^3/s) in the late afterglow. If one simply fits the $1/n_e(t)$ graph in the paper by a straight line, one obtains an upper limit of the recombination coefficient in the later afterglow of about 8×10^{-8} cm^3/s. While the data show that there is indeed something "unusual" about the decay curve, the low inferred value of $\alpha(v = 0,1) = 3 \times 10^{-7}$ cm^3/s is not sufficiently accurate to be considered a challenge to the storage ring data. In an attempt to reduce the vibrational state to $v = 0$, Smith and Špaňel carried out a second set of measurements in which they used Kr^+ ions to produce H_3^+ and, using a different fitting procedure, arrived at an even lower estimated value $\alpha(H_3^+, v = 0) \sim (1\text{–}2) \times 10^{-7}$ cm^3/s. However, the authors also found evidence that the plasma contained both H_3^+ and KrH^+ in apparent chemical equilibrium, and it is not at all obvious which of the two ions was responsible for the observed recombination loss.

Similar observations of a reduced recombination rate in the later afterglow were later made in flowing-afterglow measurements by Gougousi

et al. (1995). Given the considerable uncertainty of the data analysis, the lowest values are not in conflict with the storage ring value at 300 K. Those authors attempted to explain their observations by a three-body mechanism in which ambient electrons induce *l*-mixing in the autoionizing states. The model may have contained a kernel of truth, but it relied on unrealistically long lifetimes, taken from a merged-beam experiment, that are not supported by either theory or other measurements.

The explanation for the observed faster decay at early afterglow times may actually be that proposed by Smith and Špaňel, but in somewhat modified form. We now know from theory (Fonseca dos Santos et al., 2007) that vibrational excitation enhances recombination, even for low vibrational states. Unfortunately, there are no direct measurements of such rates that would help to put this conjecture on a firmer basis.

We conclude in this section that there are no afterglow measurements that give strong support for H_3^+ ($v = 0$) recombination coefficients significantly smaller than those found in storage rings. Those afterglow measurements, in which the state of the ion was identified by spectroscopy, consistently yielded higher values. We now turn our attention to the question why many afterglow measurements have yielded higher recombination rates.

6.2 Afterglow Measurements That Yielded High Recombination Coefficients

Most afterglow measurements, provided sufficient H_2 was present in the gas mixture, yielded recombination coefficients that were higher by factors of 2–3 than those found in the storage ring experiments. The extensive compilation of data presented in the recent paper by Glosik et al. (2009a) shows quite clearly that the observed rate coefficients tend to increase with increasing neutral density (largely helium), which suggests that the recombination is enhanced in the presence of third bodies. The problem is that the conventional three-body collisional-radiative recombination mechanisms for atomic ions, in which either neutrals or electrons act as stabilizing agents, are far too slow to explain the observed three-body rate coefficients. In the next section we will explore more efficient third-body-assisted recombination mechanisms.

6.3 Third-Body Stabilized Recombination of H_3^+

There are several possible mechanisms that could make third-body effects on recombination more efficient in the case of molecular ions that recombine indirectly via intermediate resonant states that involve capture into high Rydberg orbitals. High Rydberg states are easily

perturbed by neighboring particles, in particular the electronic angular momentum can be altered by *l*-mixing collisions and the decay by dissociation strongly depends on the electronic angular momentum. The resonant states that play a role in the binary recombination are primarily those in which the ion core is vibrationally excited by the JT interaction. Here the relevant electronic states have relatively low principal quantum numbers (around 6–8), and low angular momentum which makes predissociation fairly efficient compared to autoionization. If one assumes that all captured electrons predissociate, as is done in some simplified treatments (Jungen & Pratt, 2009), then electron capture is the rate limiting step and any additional third-body stabilization mechanism will have no effect. On the other hand, if autoionization is not negligible, then *l*-mixing by third-body interactions may lead to states that are no longer capable of autoionization, but can be stabilized by further collisions. That would enhance recombination. A mechanism of this kind was once proposed (Gougousi et al., 1995) to explain H_3^+ recombination at a time when the binary recombination mechanism was not as well established as it is now. The *l*-mixing due to electrons was thought to be the most important ingredient. In hindsight, the proposed mechanism employed unrealistically long resonance lifetimes, which were based on experimental observations in merged-beam experiments.

A different mechanism for a more efficient third-body-assisted recombination process has recently been proposed by Glosik et al. (2009a,b). It shares some features (like *l*-mixing) with the model of Gougousi et al., but it focuses on resonant states formed by capture into rotationally excited core states, which form Rydberg states with higher principal quantum number ($n = 40$–80) and invokes *l*-mixing due to ambient neutral atoms (helium in particular). These states do not usually contribute much to recombination since they tend to decay quickly by autoionization, but they can have fairly long lifetimes (e.g.>10ps) and are thus good candidates for *l*-mixing. If one now had a further mechanism that stabilizes the population of these Rydberg molecules, i.e., renders them incapable of reverting to an autoionizing state, the overall recombination rate would be enhanced and the neutral density would be one controlling factor in the recombination in the afterglow plasma. Using theoretically calculated lifetimes of the initially formed autoionizing states and estimates of the *l*-mixing efficiency due to helium atoms, and assuming that a large number of Rydberg states (principal quantum numbers from 40 to 100) contribute, the authors succeeded in deriving a three-body rate coefficient that comes close to the experimental value. However, the assumptions underlying his model are not realistic: Firstly, the authors' estimate assumes a very high *l*-mixing efficiency of the helium atoms, that is appropriate only for small principal quantum numbers, while theoretical calculations (Hickman, 1978, 1979) show that the efficiency of *l*-mixing due to helium falls off

rapidly with principal quantum number as $n^{-2.7}$ for $n > \sim 15$. Secondly, if one invokes l-mixing due to helium atoms as the rate limiting step, one should also consider l-mixing by electrons, which is known to be faster by many orders of magnitude than that due to helium atoms, and its efficiency rises with the fifth power of the principal quantum number (Dutta et al., 2001). In the range $n = 40$–80, in typical afterglows with ionization fractions of about 3×10^{-7}, l-mixing by electrons would be more efficient by factors from 10 to 10^4 than by helium atoms. Thus, one would also expect a very efficient electron-assisted recombination process, for which, however, there is little experimental evidence. The relevant rate coefficients will be discussed later. The third problem is that this model leaves unanswered the question how the l-mixed states are eventually stabilized. Collisional stabilization by stepwise n-reducing collision with either electrons or atoms may occur, but the efficiency of such collisions is not expected to be higher than for atomic systems such that the overall process is not likely to be faster than collisional radiative recombination of atomic systems.

The model also has a more basic deficiency. It focuses on the lifetime of the initially formed rotational autoionizing resonances in low l-states and then assumes that higher l-states are exclusively populated by l-mixing. A more complete model should include three-body capture of electrons into all l-states by rotationally excited H_3^+ ions and its inverse, collisional ionization. For high n-states (with binding energies below ~ 4 KT) collisional ionization occurs on a time scale that is much shorter than the time scale of recombination in an afterglow plasma such that an equilibrium population of l-mixed states is always present. Any additional l-mixing mechanism hence is of no consequence.

We will now consider a third mechanism for an efficient three-body mechanism that is an extension of the collisional dissociative process of Collins (1965), who realized that three-body capture of electrons into high Rydberg states of molecules can sometimes lead to predissociating states. Hence, the slow collisional and radiative descent from high-n to low-n states, the only stabilization route open to atomic systems, can be bypassed thus enhancing the overall recombination rate. Collins only treated a hypothetical model system with a single dissociative state, and did not consider effects of orbital angular momentum on the rate of predissociation, which should be included in a fuller treatment. In our model, we also invoke l-mixing but in the direction from high to low angular momenta and stabilization by predissociation of low l-states. We assume that in the plasma an equilibrium population of high Rydberg states, denoted by H_3^*, is maintained by three-body capture and its inverse, collisional ionization, i.e.,

$$e^- + H_3^+ + M \leftrightarrow H_3^*(n) + M \tag{21}$$

and that the equilibrium constant $K(n)$ of this reaction is approximately given by the Saha equilibrium

$$\frac{[H_3^*(n)]}{[H_3^+]n_e} = K(n) = n^2\lambda_{th}^3 e^{E_n/kT}, \tag{22}$$

where n is the principal quantum number and λ_{th} is the thermal de Broglie wavelength of the electrons at temperature T, i.e.,

$$\lambda_{th} = \frac{h^2}{(2\pi m_e kT)^{1/2}} \tag{23}$$

and E_n is the ionization potential of the Rydberg state. The assumption is made that three-body capture populates all l and magnetic substates m_l evenly. This seems justified since the inverse process, collisional ionization, depends only weakly on angular momentum of the Rydberg state. In the traditional theory of collisional radiative recombination of atomic ions, one now considers the departures from the thermal equilibrium due to the downwards collisional and radiative cascading transitions (Stevefelt et al., 1975). Under the conditions of the afterglow experiments discussed here (electron densities $<4\times10^{10}$ cm^{-3}, helium densities $<3\times10^{17}$ cm^{-3}), the effective binary rate coefficients due to either electron or helium stabilized recombination at 300 K are on the order of 10^{-9} cm^3/s, and make a negligible contribution to the binary recombination coefficient of $\sim10^{-7}$ cm^3/s. Since we are seeking a three-body mechanism that is far more efficient, we ignore all collisionally induced and radiative transitions. Instead, we focus on other mechanisms that stabilize $H_3^*(n)$. Any process, that stabilizes $H_3^*(n)$ with frequency ν_s, will enhance the overall recombination by the amount

$$\Delta\alpha(n) = K(n)\nu_s(n). \tag{24}$$

If many such states exist, the overall recombination rate will exceed the binary rate by the sum of $\Delta\alpha$ over a range of n

$$\Delta\alpha = \sum_{n_{min}}^{n_{max}} K(n)\nu_s(n), \tag{25}$$

and the effect may become comparable to the binary rate coefficient. The range of n will be discussed further below. For exploratory purposes, we assume that only s-states within a range of n predissociate on a time scale faster than l-mixing so that l-mixing becomes the rate limiting step. Let us first consider l-mixing due to electrons. It is known that electrons are very efficient in inducing l-mixing. The cross section for the process at an electron energy of 5 meV is approximately (Dutta et al., 2001)

$$\sigma'_{e,mix} = 4.4\times\pi a_0^2 n^5, \tag{26}$$

slightly smaller (by a factor of ~0.65) for electrons with thermal energy at 300 K. The corresponding rate coefficient is taken as

$$k'_{\mathrm{e,mix}} = v_{\mathrm{e}}\sigma'_{\mathrm{e,mix}}. \tag{27}$$

This rate coefficient describes the transfer from a given l,m_l state into any one of the other $n^2 - 1$ states. What we need for our purpose is the rate of transfer from any of the $n^2 - 1$ states to a particular state, namely $l = 0$, which will be smaller by the factor $1/(n^2 - 1)$. For simplicity, we take the factor as $1/n^2$.

Hence, the needed l-mixing rate $k_{\mathrm{e,mix}}$ is taken as $k'_{\mathrm{e,mix}}/n^2$ and rises with n as n^3. Inserting the relevant numbers leads to an estimate of $k_{\mathrm{e,mix}} = n^3 \times 2.7 \times 10^{-9}$ [cm^3/s]. The actual mixing rate v_{mix}, i.e., the product $n_{\mathrm{e}}\ k_{\mathrm{e,mix}}$ [1/s], is not necessarily equal to the rate limiting stabilization frequency in Equation (24), at least not for all values of n. If one made that assumption, the summation in Equation (25) would diverge strongly! One needs to take into account that the rate of predissociation of the s-states will be a declining function of n. A crude estimate may be based on the classical expectation that the rate at which an electron in an s-state will "collide" with the ion core is proportional to the classical orbiting frequency, which scales as $1/n^3$. This means that the l-mixing frequency increases as n^3, while the predissociation frequency declines as $1/n^3$. If one views l-mixing and predissociation as two "conductances" in series, the combined inductance would rise as n^3 at low n, but fall off as $1/n^3$ at high n, but we do not know *a priori* where the "crossover " might be. Experimental measurements of $H_3(n)$ predissociation spectra (Mistrík et al., 2001) show that predissociation rates of s-states fall below 10^6 [1/s] around $n = 40$, which is to be compared to the expected l-mixing rate at an electron density of 10^{10} [cm^{-3}] of about 1.7×10^6 [1/s]. The exact numbers are not critical but it seems plausible that the summation in Equation (25) should be cut off somewhere around $n = 40$. If one now performs the summation from $n_{\min} = 12$ to $n_{\max} = 40$, one finds that electron stabilized recombination makes only a fairly small contribution to the overall recombination. At the highest electron densities that are commonly used in afterglow experiments, $n_{\mathrm{e}} = 4 \times 10^{10}$ cm^{-3}, the effect would be to increase the binary rate by only about 1×10^{-8} cm^3/s, larger than the enhancement by purely collisional radiative recombination, but still only a small part of the binary rate coefficient. Our estimates indicate that the electron density will play only a minor role in typical afterglow experiments of H_3^+ recombination. This agrees with experimental observations.

The situation is quite different when one considers helium atoms as third bodies. The estimates follow very much the same scheme as for electrons, but the l-mixing rate is now taken as

$$k_{\mathrm{mix,He}} = 3.1 \times 10^{-5}\frac{1}{n^2}\frac{1}{n^{2.7}}\ [\mathrm{cm}^3/\mathrm{s}]. \tag{28}$$

This value is obtained from the cross sections given by Hickman (1978, 1979, and 1981), multiplied with the average velocity for H_3^+/He collisions at thermal energy (300 K). The fast fall-off with increasing n makes the summation in Equation (25) convergent at high n so that the high-n cutoff does not matter much. However, it is not obvious where to cut off the summation at low n. We chose a low-n cutoff at the value of n for which the ionization potential of that state exceeds thermal energy by a factor of 4 or greater. The summation then leads to the estimate that the recombination rate at $n(\mathrm{He}) = 3 \times 10^{17}$ [cm^{-3}] (10 Torr at 300K) would exceed the binary rate by 8×10^{-8} [cm^3/s] (see Figure 13). The corresponding three-body rate coefficient with helium at 300 K would be 2.6×10^{-25} [cm^6/s], which agrees with the experimental value of $(2.5 \pm 1.2) \times 10^{-25}$ [cm^6/s] (Glosik et al., 2009a), far better than one has a right to expect. The corresponding rate coefficient for D_3^+ would be $(2.2 \pm 1.2) \times 10^{-25}$ [cm^6/s], very similar to the measured values of $(1.8 \pm 0.6) \times 10^{-25}$ [cm^6/s] (Glosik et al., 2009b). Our model would predict only a small increase of the three-body coefficient at reduced temperatures, by about 50% at 100 K.

We note that helium is particularly effective in inducing l-mixing because the electron–helium momentum transfer cross section is large and nearly independent of energy. By comparison, neon should be far less effective (see Hickman, 1978). There is only a single measurement (Macdonald et al., 1984) of H_3^+ recombination in neon buffer gas (at 20 Torr) which actually yielded a significantly lower recombination rate than a very similar measurement in helium.

We also consider a third stabilization mechanism that involves the hydrogen gas that is usually present in afterglow experiments of H_3^+ recombination. It is known that H_5^+ ions recombine much more rapidly

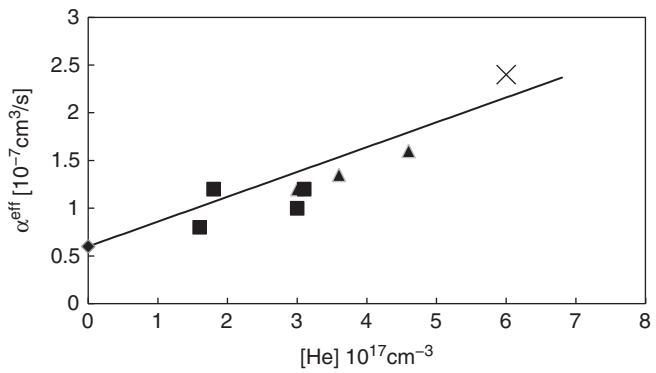

Figure 13 Observed dependence of the H_3^+ recombination coefficient at $T = 300$ K on the experimental helium density. Squares and triangles: data from Glosik (2009a). Cross: data from Leu et al. (1973). The line indicates the density dependence expected from the model described in the text

with electrons with a 300 K rate of $a(H_5^+) = 1.8 \times 10^{-6}$ [cm^3/s] (Macdonald et al., 1984). While the equilibrium concentration of H_5^+ is small compared to that of H_3^+, transient H_5^* Rydberg molecules could be formed in collisions of H_3^* with H_2, i.e., a reaction of the type

$$H_3^* + H_2 \leftrightarrow H_5^* \tag{29}$$

The forward rate coefficient should be comparable to that of fast ion–molecule reactions, i.e., $k(H_2) \sim 2 \times 10^{-9}$ cm^3/s. Once formed, these H_5^* probably predissociate very rapidly, since the recombination of H_5^+ ions is extremely fast (Macdonald et al., 1984). If one adds this as an additional stabilization mechanism to H_3^+ recombination, the effective stabilization frequency that enters Equation (24) would be given by $[H_2]k(H_2)$. The proper choice of n_{max} in the summation over n is not obvious in this case. To reproduce the large experimental value (Gougousi et al., 1995) of the three-body rate of about 2.5×10^{-23} cm^6/s, the summation would have to include n values up to about 70 and this does not seem to be unreasonable. This may also explain the rather high value obtained by Amano (1990), however, that experiment also employed very high electron densities (5×10^{11} cm^{-3}), and it is difficult to separate possible effects of electrons from those of H_2. The experiment did not show a measurable effect of H_2 on the observed recombination rate.

The foregoing estimates indicate that H_3^+ recombination in an afterglow plasma, at least in part, involves a mechanism in which the neutral gas density plays a role. This agrees with experimental findings. Helium seems to particularly effective in promoting recombination.

One would not expect a significant effect of the electron density if it is below 4×10^{10} cm^{-3}. Again, this agrees with experiments in the range of electron densities commonly present in afterglows.

The three-body model that we propose is by no means complete: The assumption that the equilibrium concentrations of the Rydberg states are only slightly perturbed is a serious simplification and ignores competition between different stabilization mechanisms. Constructing a more rigorous model, however, looks like an exceedingly complicated task.

7. COMPARISON OF STORAGE RING DATA

The storage ring measurements have yielded remarkably consistent data over the years. While some of the early measurements (Jensen, 2001; Larsson et al., 1993) gave slightly higher cross sections than was found in later work, those were shown to be due to rotational excitation of the

ions. Nearly complete control of the rotational population was eventually achieved by using either a supersonic jet expansion ion source (CRYRING) or a cryogenically cooled radio-frequency multipole trap (TSR). The actual rotational populations were verified by optical absorption measurements, and it was shown that only the two lowest rotational states were populated. As far as is known from experiment, the rotational populations in the circulating beam do not differ significantly from those injected from the ion source.

If one compares the two results obtained in the CRYRING (McCall et al., 2004) and in the TSR (Kreckel et al., 2005), one is immediately struck by the fact that the observed energy dependence is nearly identical in both experiments. It should be noted, however, that the TSR data were normalized to the CRYRING data at an energy of 10eV. The absolute magnitude of the cross sections and the overall dependence on energy are well reproduced by theory which seems to say that the binary recombination cross section has been firmly established. However, if one compares the finer structure of the measured and calculated cross sections (see Figure 14), one notices that the theoretical results show several narrow peaks that are not present in the experimental data. It is not clear at this time if this discrepancy is due to approximations made in the theory or if it indicates a possible systematic problem in the

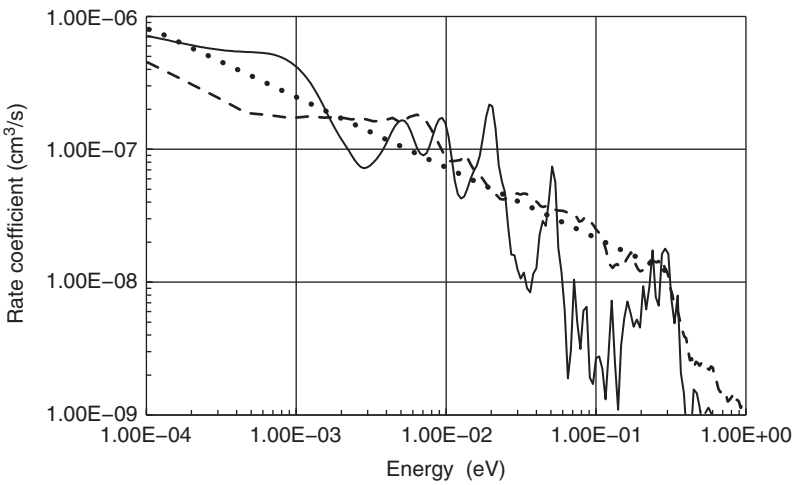

Figure 14 Comparison of the experimental CRYRING data of McCall et al. (2004) (dashed line) to the theoretical results of Fonseca dos Santos (2007) (solid line), for a rotational temperature of 13 K. The theoretical data have been convoluted with the experimental energy resolution and have been corrected for the "toroidal effect." Drawn from data supplied by M. Larsson and V. Kokoouline. The dotted line represents results of the approximate Jahn–Teller theory of Jungen and Pratt (2009)

measurements. Third-body-assisted recombination of the kind that seem to occur in afterglows can almost certainly be excluded since the relevant particle densities are lower by many orders of magnitude. Such effects have been considered in storage ring experiments of dielectronic recombination to explain the higher-than-expected recombination cross sections in the limit of very energies (Pajek and Schuch, 1997, 1999). Since DR is much faster than dielectronic recombination, it should be much less affected by third-body effects and such effects are probably negligible.

One may also ask if the magnetic field in the interaction region of storage rings (570 mT in the TSR, 300 mT in the CRYRING) and small electric stray fields (estimated to be on the order of 1 V/cm) have an effect on the recombination. Wolf et al. (2006) mention such effects without reaching a conclusion as to their importance. Several possibilities exist: If for some reason *l*-mixing due to small fields were to occur on a time scale comparable to that of autoionization or predissociation, this could affect the relative importance of the two decay channels and alter the recombination rate. If *l*-mixing should produce long-lived high-*l* states of H_3, those presumably would be field-ionized in the demerging magnets and the net effect would be that the observed recombination rate would be too small. If, on the other hand, *l*-mixing enhances the rate of predissociation, then the observed rates would come out larger than they would be in the absence of fields. One experiment (Larsson et al., 1997) et al. has been performed (for D_3^+) in which small electric fields (on the order of 30 V/cm) were deliberately added and those gave negative results. The negative finding is not totally conclusive as was mentioned by the authors of that study. Ideally one should remove all stray fields, rather than adding to them, which in practice, of course, is impossible to achieve. Some theoretical calculations have been made to assess *l*-mixing due to small static fields (Chao et al., 1998) in the context of ZEKE spectroscopy. It appears that small fields on the order of a few V/cm can induce *l*-mixing in Rydberg states, but the time constants are found to be on the order of 1–10 ns, which is much longer than likely lifetimes of H_3 autoionizing states. Hence, in the absence of evidence to the contrary, we do not believe that stray fields will have significant effects but the question may deserve further scrutiny. The same conclusion has been reached by the storage ring experimenters (Wolf, private communication).

8. H_3^+ PRODUCT BRANCHING

The first measurements of the product branching ratios

$$\begin{aligned} H_3^+ + e^- &\rightarrow H + H + H \quad (\alpha) \\ &\rightarrow H_2 + H \quad (\beta) \\ &\rightarrow H_3^* \quad (\gamma) \end{aligned} \tag{30}$$

were carried out by an extension the MEIBE merged-beam apparatus in which a grid was placed in front of the energy-sensitive detector. These experiments (Mitchell et al. 1983) were extremely challenging, suffered from fairly poor signal-to-noise ratio, and the vibrational state of the recombining ion was not known very well. Florescu-Mitchell and Mitchell (2006) provide a synopsis of the results of this work: channel α accounted for typically 52%, channel β for 40%, and surprisingly channel γ for the remaining 8%. In later work it was found that the third channel appeared to increase when the field strength in the demerging region of the experiment was reduced which seems to indicate that a fraction of the H_3^* were field-ionized in that region. If that interpretation is correct, which is still not clear at this time, then the lifetime of these metastable particles must have been on the order of or larger than about 100 ns, the flight time from the interaction region to the detector. It was this observation that motivated Gougousi et al. (1995) to propose that the recombination of H_3^+ in afterglow plasmas involved stabilization of metastable H_3^* by subsequent reactions with hydrogen molecules.

Later work by Datz et al. (1995) using the CRYRING provided more detailed and presumably more accurate energy-resolved branching fractions for H_3^+ recombination. At energies below 0.3 eV, decay channel α into three H-atoms was found to account for 75% of the total, channel β for 25 %, and channel γ was not observed at all. Datz et al. state that metastable H_3^* Rydberg molecules with principal quantum numbers below about 7 should have survived without being field-ionized while passing through the demerging magnet and hence should have been detectable. The authors concluded that formation of high Rydberg states probably does not contribute much to the recombination. The branching fractions observed by Datz et al. are very well reproduced by the statistical model of Strasser et al. (2003). Very detailed two-dimensional investigations of the kinematics of the dissociation into three H atoms and vibrational distributions of the H_2 product were also reported by Strasser et al. (2001, 2002a, and 2002b).

It is difficult to determine precise branching fractions for H_3^+ recombination afterglow measurements since there are numerous extraneous sources of H atoms. In the only such experiment (Johnsen et al., 2000) that has been performed, the H atom yield was measured by converting the H atoms to OH by reacting H with NO_2 and then measuring the OH concentration using laser-induced fluorescence. The results indicated that branch α accounts for 63% of the total, roughly compatible with the storage ring data. It was not possible to measure the H_2 yield directly or to find evidence of long-lived H_3^*.

9. ISOTOPE EFFECTS

It is difficult to perform afterglow studies of the recombination of H_2D^+ and HD_2^+, but several storage ring measurements have been published. A detailed discussion and references to theoretical papers can be found in the book by Larsson and Orel (2008). It appears that the agreement between theory and experiment is less satisfactory, especially for HD_2^+, and that more theoretical work is needed. D_3^+ has been studied by both afterglow (Glosik et al., 2009b; Gougousi et al., 1995; Laubé et al., 1998) and storage ring methods (Larsson et al., 1997). Most of the experimental data indicate that D_3^+ recombines more slowly than H_3^+ by a factor of 2–3, although one afterglow experiment (Laubé et al., 1998) gave nearly the same value for both ions. Arguing from a simplified theoretical treatment, Jungen and Pratt (2009) suggest that the recombination coefficient of D_3^+ should be smaller than that of H_3^+ by a factor of $\sqrt{2}$, a weaker isotope effects than predicted by the theory of Kokoouline and Greene (2003).

10. CONCLUSIONS

Largely motivated by applications to ionospheric physics, astrophysics, and technical applications of cold, nonequilibrium plasmas, studies of DR have been an ongoing communal effort for many years. In the case of H_3^+, results have often been difficult to reconcile, and while the discussions have been contentious at times, most often they were conducted in the spirit of collegiality, and we have now reached a state that is close to a consensus. Larsson et al. (2008), in their concise and well-presented review of the status of H_3^+ recombination studies, ask the question if "the saga has come to an end." They conclude that the "saga" is not quite finished but that it is approaching a satisfactory finale in which experiment and theory converge to a common picture of this important process. We largely concur with their assessment. As far as binary recombination is concerned, the consistency of storage ring data obtained in different experiments strongly suggests that the data are reliable and are applicable to conditions in the interstellar medium. The absolute magnitude of the coefficients is well reproduced by theory, but it would be highly desirable to refine the theoretical treatments to the point where they accurately reproduce the finer structure of the observed energy dependence of the cross section.

Larsson et al. in their review point to the outstanding problem of reconciling the afterglow and storage ring measurements, in particular those that yielded coefficients far below the binary value. We have examined the data in some detail and find that those measurements

were not performed under conditions that permit an unambiguous inference of substantially lower recombination coefficients. We also conclude that recombination in a plasma containing substantial densities of neutral and charged particles involves additional third-body-assisted mechanisms that should be taken into account in applications other than those to highly dilute interstellar media. In this we agree with the conclusion of Glosik et al. (2009a and 2009b) that neutral particles play an important part in such processes, but we propose an alternate, although still very approximate, model that seems to fit observations fairly well.

ACKNOWLEDGMENTS

The authors are indebted to several colleagues for helpful discussions, providing alternate viewpoints, and providing data files, in particular to M. Larsson, S. Kokoouline, J. Glosik, A. Wolfe, and C. Greene. SLG gratefully acknowledges support from the US National Science Foundation under grant ATM-0838061. This research is also supported by NASA Grants NNX08AE67G and NNX09AQ73G.

SLG dedicates this chapter to the memory of his beloved wife and precious companion, Susan L. Greenblatt, who in spite of her serious illness continued to encourage this work but unfortunately did not live to see its completion.

REFERENCES

Adams, N. G., Smith, D., and Alge, E. (1984). Measurements of dissociative recombination coefficients of H_3^+, HCO^+, N_2H^+, and CH_5^+ at 95 and 300 K using the FALP apparatus. *The Journal of Chemical Physics*, *81*(4), 1778–1784.

Amano, T. (1988). Is the dissociative recombination of H_3^+ really slow? A new spectroscopic measurement of the rate constant. *Astrophysical Journal Letters*, *329*, L121–L124.

Amano, T. (1990). The dissociative recombination rate coefficients of H_3^+, HN_2^+, and HCO^+. *The Journal of Chemical Physics*, *92*(11), 6492–6501.

Amitay, Z., Zajfman, D., Forck, P., Hechtfischer, U., Seide, B., Grieser, M., , Habs, D., Repnow, R., Schwalm, D., & Wolf, A., (1996). "Dissociative recombination of CH+: Cross section and final states". *Physical Review A - Atomic, Molecular, and Optical Physics*, vol. *54*, no. 5, pp. 4032–4050.

Auerbach, D., Cacak, R., Caudano, R., Gaily, T. D., Keyser, C. J., McGowan, J. W., et al. (1977). Merged electron-ion beam experiments. I. Method and measurements of (e-H2+) and (e-H_3^+) dissociative-recombination cross sections. *Journal of Physics B: Atomic and Molecular Physics*, *10*(18), 3797–3820.

Bardsley, J. N. (1968). The theory of dissociative recombination. *Journal of Physics B*, *1*, 365.

Bates, D. R. (1950). Dissociative recombination. *Physical Review*, *78*, 492.

Bates, D. R., Guest, M. F., & Kendall, R. A. (1993) Enigma of H_3^+dissociative recombination. *Planetary and Space Science*, *41*(1), 9–15.

Canosa, A., Gomet, J. C., Rowe, B. R., Mitchell, J. B. A., & Queffelec, J. L. (1992). Further measurements of the H_3^+(v = 0,1,2) dissociative recombination rate coefficient. *The Journal of Chemical Physics*, *97*(2), 1028–1037.

Cencek, W., Rychlewski, J., Jaquet, R., & Kutzelnigg, W. (1998). "Sub-microhartree accuracy potential energy surface for H3+ including adiabatic and relativistic effects. I. Calculation of the potential points", *The Journal of Chemical Physics*, *108*, 2831.

Chao, S. D., Hayashi, M., Lin, S. H., & Schlag, E. W. (1998). *l*-mixing dynamics of Rydberg states of hydrogen atom in a static electric field. *Journal of Physics B: Atomic, Molecular and Optical Physics*, *31*(9), 2007–2021.

Collins, C. B. (1965). Collisional-dissociative recombination of electrons with molecular ions. *Physical Review*, *140*(6A), A1850–A1857.

Cunningham, A. J., O'Malley, T. F., & Hobson, R. M. (1981). On the role of vibrational excitation in dissociative recombination., *Journal of Physics B: Atomic and Molecular Physics*, *14*(4), 773–782.

Datz, S., Sundström, G., Biedermann, C., Broström, L., Danared, H., Mannervik, S., et al. (1995a). Branching processes in the dissociative recombination of H_3^+. *Physical Review Letters*, *74*(6), 896–899.

Datz, S., Sundström, G., Biedermann, C., Broström, L., Danared, H., Mannervik, S., et al. (1995b). Erratum: Branching processes in the dissociative recombination of H_3^+. *Physical Review Letters*, *74*(20), 4099.

Dutta, S. K., Feldbaum, D., Walz-Flannigan, A., Guest, J. R., & Raithel, G. (2001). High-angular-momentum states in cold Rydberg gases. *Physical Review Letters*, *86*(18), 3993–3996.

Flannery, M. R. (1995). The semiclassical-classical path theory of direct electron-ion dissociative recombination and e- + H_3^+ recombination. *International Journal of Mass Spectrometry and Ion Processes*, *149–150*(C), 597–607.

Florescu-Mitchell, A. I., & Mitchell, J. B. A. (2006). Dissociative recombination. *Physics Reports*, *430*(5–6), 277–374.

Fonseca dos Santos, S., Kokoouline, V., & Greene, C. H. (2007). Dissociative recombination of H_3^+ in the ground and excited vibrational states. *The Journal of Chemical Physics*, *127*, 124309.

Giusti, A. (1980). A multichannel quantum defect theory approach to dissociative recombination. *Journal of Physics B*, *13*, 3867–3894.

Glosík, J., Plašil, R., Korolov, I., Dohnal, P., Novotný, O., Varju, J., Roučka, Š., Greene, C. H., Kokoouline, V., (2009b). Binary and ternary recombination of D_3^+ ions with electrons in He-D2 plasma. *Physical Review A, Atomic, Molecular and Optical Physics*, *80*, 042706-1–042706-7

Glosík, J., Plašil, R., Korolov, I., Kotrík, T., Novotný, O., Hlavenka, P., et al. (2009a). Temperature dependence of binary and ternary recombination of H_3^+ ions with electrons. *Physical Review A – Atomic, Molecular, and Optical Physics*, *79*, 052707-1–052707-10

Gougousi, T., Johnsen, R., & Golde, M. F. (1995). Recombination of $H_3^+$and D_3^+ ions in a flowing afterglow plasma. *International Journal of Mass Spectrometry and Ion Processes*, *149–150*(C), 131–151.

Greene, C. H., Kokoouline, V., & Esry, B. D. (2003). Importance of Jahn-Teller coupling in the dissociative recombination of H_3^+ by low energy electrons. In S. L. Guberman (Ed.), *Dissociative recombination of molecular ions with electrons* (pp. 221–233). New York: Kluwer Academic/ Plenum Publishers.

Guberman, S. L. (1994). Dissociative recombination without a curve crossing. *Physical Review A*, *49*(6), R4277–R4280.

Guberman, S. L. (1995). Recent theoretical developments in dissociative recombination. In *Atomic collisions: A symposium in honor of Christopher Bottcher (1945–1993)* ed. by D. R. Schultz, M. R. Strayer and J. H. Macek (p. 88). New York: American Institute of Physics Press.

Guberman, S. L. (1997). Mechanism for the green glow of the upper ionosphere. *Science*, *278*, 1276–1278.

Guberman, S. L. (2007). Role of excited core Rydberg states in dissociative recombination. *Journal of Physical Chemistry A*, *111*(44), 11254–11260.

Guberman, S. L., & Giusti-Suzor, A. (1991). The generation of O(^{1}S) from the dissociative recombination of O_2^+. *Journal of Chemical Physics*, *95*, 2602.

Herbst, E. (2007). Molecular ions in interstellar networks. *Journal of Physics: Conference Series*, *4*, 17–25.

Herzberg, G. (1945). *Molecular spectra and molecular structure, II infrared and Raman spectra of polyatomic molecules* (pp. 84). Princeton, NJ: D. van Nostrand Co. Inc.

Herzberg, G. (1966). *Molecular spectra and molecular structure, III electronic spectra and electronic structure of polyatomic molecules* (pp. 40–65). Princeton, NJ: D. van Nostrand Co. Inc.

Hickman, A. P. (1978). Theory of angular momentum mixing in Rydberg-atom-rare-gas collisions. *Physical Review A*, *18*(4), 1339–1342.

Hickman, A. P. (1979). Relation between low-energy-electron scattering and *l*-changing collisions of Rydberg atoms. *Physical Review A*, *19*(3), 994–1003.

Hickman, A. P. (1981). The effect of core interactions in *l*-mixing collisions of Rydberg atoms with rare gases. *Journal of Physics B: Atomic and Molecular Physics*, *14*(13), L419–L424.

Hickman, A. P. (1987). Dissociative recombination of electrons with H_2^+. *Journal of Physics B*,*20*, 2091.

Hus, H., Youssif, F., Sen, A., & Mitchell, J. B. A. (1988). Merged-beam studies of the dissociative recombination of H_3^+ ions with low internal energy. *Physical Review A*, *38*(2), 658–663.

Jahn, H. A., & Teller, E. (1937). Stability of polyatomic molecules in degenerate electronic states. I. Orbital degeneracy. *Proceedings of the Royal Society A*, *161*, 220–235.

Jaquet, R., Cencek, W., Kutzelnigg, W., & Rychlewski, J. (1998). "Sub-microhartree accuracy potential energy surface for H3+ including adiabatic and relativistic effects. II. Rovibrational analysis for H3+ and D3+". *The Journal of Chemical Physics*, *108*, 2837.

Jensen, M. J., Pedersen, H. B., Safvan, C. P., Seiersen, K., Urbain, X., & Andersen, L. H. (2001). Dissociative recombination and excitation of H_3^+. *Physical Review A. Atomic, Molecular, and Optical Physics*, *63*(5), 527011–527015.

Johnsen, R. (1987). Microwave afterglow measurements of the dissociative recombination of molecular ions with electrons. *International Journal of Mass Spectrometry and Ion Processes*, *81*(C), 67–84.

Johnsen, R. (2005). A critical review of H_3^+ recombination studies. *Journal of Physics: Conference Series*, *4*, 83–89.

Johnsen, R., & Mitchell, J. B. A. (1998). Complex formation in electron-ion recombination of molecular ions. *Advances in Gas Phase Ion Chemistry*, *3*, 49–80.

Johnsen, R., Skrzypkowski, M., Gougousi, T., & Golde M. F. (2000). Spectroscopic emissions from the recombination of N_2O^+, N_2OH^+/HN_2O^+, CO_2^+ , CO_2H^+, HCO^+/COH^+, H_2O^+, NO_2^+, HNO^+, and LIF measurements of the H atom yield from H_3^+. In M. Larsson, J. B. A. Mitchell, & I. F. Schneider (Eds.), *Dissociative recombination, theory, experiment, and applications*. Singapore: World Scientific Publishing.

Jungen, C., & Pratt, S. T. (2009). Jahn-Teller interactions in the dissociative recombination of H_3^+. *Physical Review Letters*, *102*(2), 023201-1–023201-4.

Jungen, Ch. (1996). *Molecular applications of quantum defect theory*. Bristol: Institute of Physics Publishing.

Kokoouline, V., & Greene, C. H. (2003a). Theory of dissociative recombination of D_{3h} triatomic ions applied to H_3^+. *Physical Review Letters*, *90*(13), 133201-1–133201-4.

Kokoouline, V., & Greene, C. H. (2003b). Unified theoretical treatment of dissociative recombination of D3h triatomic ions: Application to $H_3^+$and D_3^+. *Physical Review A – Atomic, Molecular, and Optical Physics*, *68*(1), 012703-1–012703-23.

Kokoouline, V., & Greene, C. H. (2005). Theoretical study of the H_3^+ ion dissociative recombination process. *Journal of Physics: Conference Series*, *4*, 74–82.

Kokoouline, V., Greene, C. H., & Esry, B. D. (2001). Mechanism for the destruction of H_3^+ ions by electron impact [3]. *Nature*, *412*(6850), 891–894.

Kreckel, H., Motsch, M., Mikosch, J., Glosík, J., Plasil, R., Altevogt, S., et al. (2005). High-resolution dissociative recombination of cold H_3^+ and first evidence for nuclear spin effects. *Physical Review Letters*, *95*(26), 1–4.

Kulander, K. C., & Guest, M. F. (1979). Excited electronic states of H_3 and their role in the dissociative recombination of H_3^+. *Journal of Physics B: Atomic and Molecular Physics*, *12*, L501–L504.

Lampert, A., Wolf, A., Habs, D., Kenntner, J., Kilgus, D., Schwalm, D., et al. (1996), High-resolution measurement of the dielectronic recombination of fluorinelike selenium ions. *Physical Review A*, *53*, 1413.

Larsson, M., Danared, H., Larson, Å., Le Padellec, A., Peterson, J. R., Rosén, S., et al. (1997). Isotope and electric field effects in dissociative recombination of D_3^+. *Physical Review Letters*, *79*(3), 395–398.

Larsson, M., Danared, H., Mowat, J. R., Sigray, P., Sundström, G., Broström, L., et al. (1993). Direct high-energy neutral-channel dissociative recombination of cold H3+ in an ion storage ring. *Physical Review Letters*, *70*(4), 430–433.

Larsson, M., McCall, B. J., & Orel, A. E. (2008). The dissociative recombination of H_3^+ – a saga coming to an end? *Chemical Physics Letters*, *462*(4–6), 145–151.

Larsson, M., & Orel, A. E. (2008). *Dissociative recombination of molecular ions*. Cambridge: Cambridge University Press.

Laubé, S., Le Padellec, A., Sidko, O., Rebrion-Rowe, C., Mitchell, J. B. A., and Rowe, B. R. (1998). New FALP-MS measurements of H_3^+, $D_3^+$and HCO^+ dissociative recombination. *Journal of Physics B: Atomic, Molecular and Optical Physics*, *31*(9), 2111–2128.

Lee, C. M. (1977). Multichannel dissociative recombination theory. *Physical Review A*, *16*, 109–122.

Leu, M. T., Biondi, M. A., and Johnsen, R. (1973). Measurements of recombination of electrons with H_3^+ and H_5^+ ions. *Physical Review A*, *8*(1), 413–419.

Lin, C. D. (1995). Hyperspherical coordinate approach to atomic and other coulombic three-body systems. *Physics Reports*, *257*, 1–83.

Macdonald, J. A., Biondi, M. A., & Johnsen, R. (1984). Recombination of electrons with H_3^+ and H_5^+ ions. *Planetary and Space Science*, *32*(5), 651–654.

Macko, P., Bánó, G., Hlavenka, P., Plašil, R., Poterya, V., Pysanenko, A., et al. (2004). Afterglow studies of $H_3^+(v=0)$ recombination using time resolved cw-diode laser cavity ring-down spectroscopy. *International Journal of Mass Spectrometry*, *233*(1–3), 299–304.

McCall, B. J. (2006). Dissociative recombination of cold H_3^+ and its interstellar implications. *Philosophical Transactions of the Royal Society A: Mathematical, Physical and Engineering Sciences*, *364*(1848), 2953–2963.

McCall, B. J., Hinkle, K. H., Geballe, T. R., Moriarty-Schieven, G. H., Evans II, N. J., Kawaguchi, K., Takano, S., Smith, V. V., Oka, T., et al. (2002). Observations of H_3^+ in the diffuse interstellar medium. *Astrophysical Journal*, vol. 567 no. 1. pp. 391–406.

McCall, B. J., Huneycutt, A. J., Saykally, R. J., Djuric, N., Dunn, G. H., Semaniak, J., et al. (2004). Dissociative recombination of rotationally cold H_3^+. *Physical Review A – Atomic, Molecular, and Optical Physics*, *70*(5A), pp. 052716-1–052716-12.

McCall, B. J., Huneycutt, A. J., Saykally, R. J., Djuric, N., Dunn, G. H., Semaniak, J., Novotny, O., Al-Khalili, A., Ehlerding, A., Hellberg, F., Kalhori, S., Neau, A., Thomas, R. D., Paal, A., O¨sterdah, A. A., & Larsson, M., (2004). "Dissociative recombination of rotationally cold H_3^+". *Physical Review A - Atomic, Molecular, and Optical Physics*, vol. *70*, no. 5A, pp. 052716-1–052716-12.

Michels, H. H., & Hobbs, R. H. (1984). Low temperature dissociative recombination of $H_3^+ + e^-$. *Astrophysics Journal*, *286*, L27.

Mistrík, I., Reichle, R., Helm, H., & Müller, U. (2001). Predissociation of H_3 Rydberg states. *Physical Review A – Atomic, Molecular, and Optical Physics*, *63*(4), 042711-1–042711-11

Mistrík, I., Reichle, R., Müller, U., Helm, H., Jungen, M., & Stephens, J. A. (2000). Ab initio analysis of autoionization of H_3 molecules using multichannel quantum-defect theory and new quantum-defect surfaces. *Physical Review A – Atomic, Molecular, and Optical Physics*, *61*(3), 334101–3341016.

Mitchell, J. B. A., Forand, J. L., Ng, C. T., Levac, D. P., Mitchell, R. E., Mul, P. M., et al. (1983). Measurement of the branching ratio for the dissociative recombination of $H_3^+ + e$. *Physical Review Letters*, *51*(10), 885–888.

Mitchell, J. B. A., & Rogelstad, M. R. (1996). In D. Zajfman, J. B. A. Mitchell, D. Schwalm, & B. R. Rowe (Eds.), *Dissociative recombination: Theory, experiment, and applications*. Singapore: World Scientific.

Nakashima, K., Takagi, H., & Nakamura, H. (1987). Dissociative recombination of H_2^+, HD^+, and D_2^+ by collisions with slow electrons. *The Journal of Chemical Physics*, *86*(2), 726–737.

Nager, C., & Jungen, M. (1982). Potential surfaces for the Rydberg states of H_3. *Chemical Physics*, *70*(3), 189–198.

O'Malley, T. F. (1966). Theory of dissociative attachment. *Physical Review A*, *150*, 14–29.

O'Malley, T. F. (1981). Rydberg levels and structure in dissociative recombination cross sections. *Journal of Physics B*, *14*, 1229.

Pajek, M., & Schuch, R. (1997). Three-body recombination of ions with electrons in cooler-storage rings. *Hyperfine Interactions*, *108*(1–3), 185–194.

Pajek, M., & Schuch, R. (1999). Plasma effects in three-body recombination of high-Z bare ions with electrons. *Physica Scripta T*, *80*(B), 307–309.

Pan, F.-S., & Oka, T. (1986). Calculated forbidden rotational spectra of H_3^+. *Astrophysics Journal*, *305*, 518–525.

Peart, B., & Dolder, K. T. (1974). Measurements of the dissociative recombination of H_3^+ ions. *Journal of Physics B: Atomic and Molecular Physics*, *7*(14), 1948–1952.

Petsalakis, I. D., Theodorakopoulos, G., & Wright, J. S. (1988). Theoretical calculations on electronic transitions for H_3, including Rydberg and transition state spectra. *The Journal of Chemical Physics*, *89*(11), 6850–6859.

Pineau Des Forêts, G., & Roueff, E. (2000). H_3^+ recombination and bistability in the interstellar medium. *Philosophical Transactions of the Royal Society A: Mathematical, Physical and Engineering Sciences*, *358*(1774), 2549–2559.

Plašil, R., Glosík, J., Poterya, V., Kudrna, P., Rusz, J., Tichý, M., et al. (2002). Advanced integrated stationary afterglow method for experimental study of recombination of processes of H_3^+ and D_3^+ ions with electrons. *International Journal of Mass Spectrometry*, *218*(2), 105–130.

Sarpal, B., Tennyson, J., & Morgan, L. A. (1994). Dissociative recombination without crossing: Study of HeH^+. *Journal of Physics B*, *27*, 5943.

Schneider, I., & Orel, A. E. (1999). Accurate nonadiabatic couplings for H_3: Application to predissociation. *Journal of Chemical Physics*, *111*, 5873.

Schneider, I. F., Orel, A. E., & Suzor-Weiner, A. (2000). Channel mixing effects in the dissociative recombination of H_3^+ with slow electrons. *Physical Review Letters*, *85*(18), 3785–3788.

Schneider, I., Strömholm, C., Carata, L., Urbain, X., Larsson, M., & Suzor-Weiner, A. (1997). Rotational effects in HD^+ dissociative recombination: theoretical study of resonant mechanisms and comparison with ion storage ring experiments. *Journal of Physics B*, *30*, 2687–2705.

Shaad, L. J., & Hicks, W. V. (1974). Gaussian basis configuration interaction calculations on twenty electronic states of ~~H3+~~ H3+. A bound ~~3Σu+~~ $^3\Sigma u^+$ excited level. *The Journal of Chemical Physics*, *61*, 1934.

Siegbahn, P., & Liu, B. (1978). An accurate three-dimensional potential energy surface for ~~H3~~ H3. *The Journal of Chemical Physics*, *68*, 2457.

Seaton, M. J. (1983). Quantum defect theory. *Reports of Progress in Physics*, *46*, 167–257.

Skrzypkowski, M. P., Johnsen, R., Rosati, R. E., & Golde, M. F. (2004). Flowing-afterglow measurements of collisional radiative recombination of argon ions. *Chemical Physics*, *296*(1), 23–27.

Smith, D., & Špaňel, P. (1993). Dissociative recombination of H_3^+. Experiment and theory reconciled. *Chemical Physics Letters*, *211*(4–5), 454–460.

Staib, A., & Domcke, W. (1990). Analysis of the Jahn-Teller effect in the np^2E' Rydberg series of H_3 and D_3. *Zeitschrift fur Physik D*, *16*, 275–282.

Stevefelt, J., Boulmer, J., & Delpech, J.-F. (1975). Collisional-radiative recombination in cold plasmas. *Physical Review A*, *12*(4), 1246–1251.

Strasser, D., Lammich, L., Kreckel, H., Krohn, S., Lange, M., Naaman, A., et al. (2002a). Breakup dynamics and the isotope effect in H_3^+ and D_3^+dissociative recombination. *Physical Review A – Atomic, Molecular, and Optical Physics*, *66*(3), 327191–3271913.

Strasser, D., Lammich, L., Krohn, S., Lange, M., Kreckel, H., Levin, J., et al. (2001). Two- and three-body kinematical correlation in the dissociative recombination of H_3^+. *Physical Review Letters*, *86*(5), 779–782.

Strasser, D., Levin, J., Heber, O., Wolf, A., Wolf, A., Schwalm, D., and Zajfman, D., (2003). "A model for calculating branching ratios in H_3^+ dissociative recombination" in "Dissociative recombination of molecular ions with electrons", ed.Guberman, S.L., 2003 Kluwer Academic/Plenum Publishers.

Strömholm, C., Stemaniak, J., Rosén, S., Danared, H., Datz, S., van der Zande, W., et al. (1996) Dissociative recombination and dissociative excitation of ^{4}HeH: Absolute cross sections and mechanisms. *Physical Review*, *A54*, 3086.

Sundström, G., Mowat, J. R., Danared, H., Datz, S., Broström, L., Filevich, A., et al. (1994). Destruction rate of H_3^+ by low-energy electrons measured in a storage-ring experiment. *Science*, *263*(5148), 785–787.

Takagi, H., (1993). Rotational effects in the dissociative recombination process of H_2^+ e. *Journal of Physics B*, *26*, 4815–4832.

Takagi, H. (2003). Extension of the quantum defect theory and its application to electron and molecular ion collisions. In S. L. Guberman (Ed.), *Dissociative recombination of molecular ions with electrons* (pp. 177–186). New York: Kluwer Academic/ Plenum Publishers.

Takagi, H., Kosugi, N., and Le Dourneuf, M. (1991). Dissociative recombination of CH^+, Journal of Physics B, Atomic, Molecular and Optical Physics, 24 , 711–732.

Tashiro, M., & Kato, S. (2002). Quantum dynamics study on predissociation of H_3 Rydberg states: Importance of indirect mechanism. *The Journal of Chemical Physics*, *117*(5), 2053–2062.

Tashiro, M., & Kato, S. (2003). Quantum dynamical study of H_3^+ recombination. In S. L. Guberman (Ed.), *Dissociative recombination of molecular ions with electrons* (pp. 243–248). New York: Kluwer Academic/Plenum Publishers.

Tom, B. A., Zhaunerchyk, V., Wiczer, M. B., Mills, A. A., Crabtree, K. N., Kaminska, M., et al. (2009). Dissociative recombination of highly enriched para-H_3^+. *Journal of Chemical Physics*, *130*(3), pp. 031101-1–031101-4.

Truhlar, D. G., & Horowitz, C. J. (1978). Functional representation of Liu and Siegbahn's accurate ab inito potential energy calculations for H+H2. *The Journal of Chemical Physics*, *68*, 2466.

Varandas, A. J. C., Brown, F. B., Mead, C. A., Truhlar, D. G., & Blais, N. C. (1987). A double many-body expansion of the two lowest-energy potential surfaces and nonadiabatic coupling for H3. *The Journal of Chemical Physics*, *86*, 6258.

Watson, J. K. G. (2000). An introduction to the spectroscopy of H3+. *Philosophical Transactions of the Royal Society of London*, *358*, 2371–2384.

Wolf, A., Kreckel, H., Lammich, L., Strasser, D., Mikosch, J., Glosík, J., et al. (2006). Effects of molecular rotation in low-energy electron collisions of H3 +. *Philosophical Transactions of the Royal Society A: Mathematical, Physical and Engineering Sciences*, *364*(1848), 2981–2997.